American Mineralogist, Volume 100, pages 1277–1303, 2015

Review

Routine characterization and interpretation of complex alkali feldspar intergrowths† 🔓

Ian Parsons[1,*], John D. Fitz Gerald[2] and Martin R. Lee[3]

[1]Grant Institute of Earth Science, University of Edinburgh, James Hutton Road, Edinburgh, EH9 3FE, U.K.
[2]Research School of Earth Sciences, Australian National University, Canberra, ACT 0200, Australia
[3]School of Geographical and Earth Sciences, University of Glasgow, Lilybank Gardens, Glasgow, G12 8QQ, U.K.

Abstract

Almost all alkali feldspar crystals contain a rich inventory of exsolution, twin, and domain microtextures that form subsequent to crystal growth and provide a record of the thermal history of the crystal and often of its involvement in replacement reactions, sometimes multiple. Microtextures strongly influence the subsequent behavior of feldspars at low temperatures during diagenesis and weathering. They are central to the retention or exchange of trace elements and of radiogenic and stable isotopes. This review is aimed at petrologists and geochemists who wish to use alkali feldspar microtextures to solve geological problems or who need to understand how microtextures influence a particular process. We suggest a systematic approach that employs methods available in most well founded laboratories. The crystallographic relationships of complex feldspar intergrowths were established by the 1970s, mainly using single-crystal X-ray diffraction, but such methods give limited information on the spatial relationships of the different elements of the microtexture, or of the mode and chronology of their formation, which require the use of microscopy. We suggest a combination of techniques with a range of spatial resolution and strongly recommend the use of orientated sections. Sections cut parallel to the perfect (001) and (010) cleavages are the easiest to locate and most informative. Techniques described are light microscopy; scanning electron microscopy using both backscattered and secondary electrons, including the use of surfaces etched in the laboratory; electron-probe microanalysis and analysis by energy-dispersive spectrometry in a scanning electron microscope; transmission electron microscopy. We discuss the use of cathodoluminescence as an auxiliary technique, but do not recommend electron-backscattered diffraction for feldspar work. We review recent publications that provide examples of the need for great care and attention to pre-existing work in microtextural studies, and suggest several topics for future work.

Keywords: Chemical diffusion, diffraction, fluids in the crust (special collection), mineral physics, nanoscale

Introduction

Alkali feldspar is the third most abundant mineral in Earth's crust. With the exception of rare, very rapidly cooled volcanic alkali feldspars and some near end-member crystals that grew at diagenetic temperatures, almost all natural alkali feldspar crystals exhibit various intracrystal exsolution and twin microtextures that developed during their geological history. These microtextures provide a rich source of information on crystal growth *T*, cooling rates, and isochemical and non-isochemical replacement reactions with late magmatic or externally derived aqueous fluids. They can be used to identify regions of crystals that have been unaffected by fluids since original growth and which can therefore be reliably selected to explore magmatic and metamorphic processes using microbeam chemical analysis. Replacive microtextures are associated with micropores that cause turbidity and from which fluids can be extracted. The chronology and *T* of multiple phases of replacement, and possible accompanying changes in bulk rock composition, can be established. In sedimentary rocks microtextures in detrital feldspar grains can be used as provenance indicators. They guide diagenetic dissolution, leading to secondary porosity formation, and diagenetic replacement. Microtextures are responsible for the rapid dissolution and mechanical degradation of feldspar during soil formation, and the intricate grain surfaces that are created may have provided protective reactors for the origin of life. Defects govern the rate of ^{40}Ar loss from alkali feldspars over geological time and the release of Ar during laboratory step heating, and they define the reactivity of feldspars with respect to ^{16}O-^{18}O exchange and many other geochemically important processes.

Alkali feldspar microtextures have been investigated by many techniques. Their known complexity has increased over many years, reaching its current apogee in feldspars from the Klokken intrusion (Fig. 2; Parsons et al. 2013) that contain at least eight chemically distinct phases, some of them twinned in up to four orientations. The present review is designed for petrologists and geochemists. We introduce basic terminol-

* E-mail: ian.parsons@ed.ac.uk
† 🔓 Open access: Article available to all readers online.

0003-004X/15/0506–1277$05.00/DOI: http://dx.doi.org/10.2138/am-2015-5094

ogy, phase relationships, and phase behavior, and we describe the processes that occur in cooling feldspars to produce their microtextural diversity. We review critically the ways in which microtextures can contribute to the understanding of geological and geochemical processes. We then suggest the most effective ways of characterizing and interpreting common microtextures, over a large range of scales, using widely available methods, and draw special attention to the advantages of using orientated samples. There is little here that is new but we bring together elements of interpretation and techniques that are disseminated through a large and diverse literature. In a final section we review some recent papers on alkali feldspar microtextures (Balić-Žunić et al. 2013; Yuguchi and Nishiyama 2007; Yuguchi et al. 2011a, 2011b) that highlight the importance of studying microtextures at a range of scales in orientated sections, and the value of the considerable body of previous work that exists in the literature, if incorrect conclusions are to be avoided.

As a vehicle to introduce methods of characterization, we draw mainly on our own published work, particularly on alkali feldspars from the hyper-solvus Klokken syenite intrusion in the Gardar province of South Greenland and the sub-solvus Shap granite from Northwest England, which we refer to simply as Klokken and Shap. Their microtextures are summarized in Figures 1 and 2, but we strongly recommend viewing the original micrographs in the papers we cite below. From a microtextural standpoint these are arguably the most intensively studied plutonic alkali feldspars and both provide examples of microtextures formed by volume diffusion and by multiple phases of replacement in aqueous fluids. It is important not to generalize their features too widely but we have seen similar features in many other examples of syenitic and granitic rocks. Other workers, some cited below, have reported comparable features. Each alkali feldspar can potentially record a different history, especially with respect to replacive events, and many other types of microtexture are known, particularly in pegmatites (Smith and Brown 1988; Cerný 1994; Parsons and Lee 2005; Sánchez-Muñoz et al. 2012) and granulite facies rocks (Waldron et al. 1993; Cayzer 2002; Parsons and Lee 2005; Abart et al. 2009b; Tajčmanová et al. 2012). Many perthitic intergrowths are described by Smith and Brown (1988, Ch. 19) and a library of images is provided by Parsons et al. (2005). Relevant phase diagrams can be downloaded freely in poster form from www.minersoc.org/files/feldspar-1.pdf (also /feldspar-2.pdf) and background information for these posters is provided by Parsons (2010).

Evolution and terminology of techniques

Perthitic intergrowths are composed of two or more feldspar phases within the outline of a single alkali feldspar crystal. They were initially studied by light microscopy (LM) (e.g., Alling 1921, 1932; Andersen 1928). LM can be employed using plane-polarized light (PPL) or crossed polarizers (XP). Single-crystal X-ray diffraction (SXRD) was introduced very successfully by Smith and MacKenzie (1955) and the character of a large range of intergrowths established (see review by MacKenzie and Smith 1962). When computers became widely available cell parameters could be refined routinely from powder diffraction measurements (PXRD) (e.g., Stewart and Wright 1974). Although these methods are effective for identifying the feldspar phases present in a sample, and in the case of SXRD, the orientation of elements of the microtexture including twinning, they do not provide information on the spatial relationships and chronology of the microtexture. For this purpose transmission electron microscopy (TEM) has proved most rewarding. This approach is not new; beautiful images of complex textures in cryptoperthites similar to those from Klokken were obtained by Lorimer and Champness (1973) and TEM techniques and other pioneering work were reviewed by McLaren (1974). A major advantage of TEM is that electron diffraction patterns can be obtained from selected areas of the image (SAED). The crystal lattice can be imaged using high-resolution TEM (HRTEM) but not the crystal structure. TEM is often carried out in conjunction with scanning electron microscopy (SEM), which bridges the gap between the LM and TEM scales. SEM images can be obtained in both secondary electron (SE) and backscattered electron modes (BSE), when the image is formed by mean atomic number contrast (Z-contrast). A promising new SEM technique, charge contrast imaging (CCI), has recently been introduced by Flude et al. (2012). Electron backscatter diffraction (EBSD) patterns can also be obtained in an SEM. Cathodoluminescence (CL) images can be obtained using detectors fitted to light and scanning electron microscopes and can reveal microtextures related to the distribution of trace elements and point defects that are otherwise difficult to detect.

Electron microprobe microanalysis (EPMA), with a small diameter beam, can be used to obtain phase compositions at scales greater than a few micrometers, and bulk compositions of regions with fine-scale intergrowths can be obtained using a defocussed beam or of whole crystals by traversing. Chemical analysis by energy-dispersive spectroscopy (EDS) can be carried out with an SEM at similar scales. Analytical TEM (ATEM) can provide phase analyses at scales of ~150 nm. Major element distributions can be mapped at extremely small scale (<100 nm) in TEMs fitted with electron-energy-selecting column optics (energy-filtered TEM, EFTEM). Laser-ablation inductively coupled mass-spectrometry (LA-ICPMS), with laser beams of ~20 μm diameter, has been used to study the distribution of trace elements with respect to perthitic microtextures as has the ion-microprobe (secondary-ion mass spectrometry, SIMS).

The techniques listed above are those most likely to be used for characterization of intracrystal microtextures and below we describe those most profitably used for routine work. Many other techniques have been used to study feldspars, including neutron diffraction, nuclear magnetic resonance, Raman spectroscopy, Fourier-transform infrared spectroscopy (FTIR), and X-ray absorption spectroscopy, using synchrotron sources. These and other techniques are described in Smith and Brown (1988), and techniques related to the chemistry and structure of feldspar surfaces, including atomic force microscopy (AFM), are summarized by Smith (1994).

Terminology related to microtextures

This section introduces basic terminology. Several items are expanded in later sections. The words microtexture and microstructure are often used interchangeably, but we here reserve microstructure for features at or near the atomic scale, involving at most a few unit cells. Alling (1921) recognized that perthitic intergrowths formed by exsolution of a homogeneous alkali feldspar, following magmatic crystallization, and also

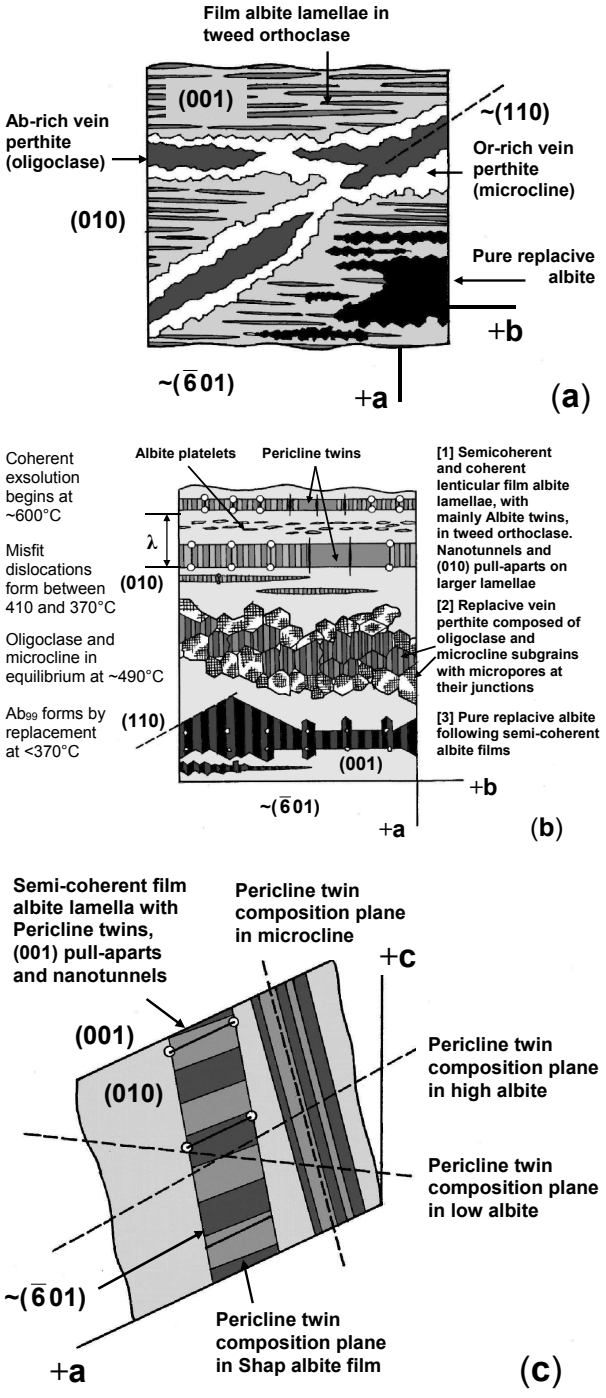

◀**FIGURE 1.** Cartoons illustrating microtextures in alkali feldspar phenocrysts in the Shap granite. See text for supporting micrographs. Each drawing shows features visible in cleavage fragments (or in similarly orientated thin sections) resting on the best-developed cleavages, (001) (**a**,**b**) and (010) (**c**), with outlines defined by the second cleavage and the "Murchison plane," near ($\bar{6}$01). Shades of gray approximate to composition as they appear in BSE images: Or-rich feldspar is white or pale gray, Ab-rich feldspar is black or dark gray. Shades of gray are also used to indicate Albite and Pericline twins but the twins do not differ in composition. Angular relationships are drawn accurately but considerable liberties have been taken with relative scales, which cover a very large range. (**a**) Features visible in a (001) thin section using LM. Film albite lamellae occur in non-turbid regions and usually have periodicities in the range 5–1 μm and maximum thicknesses of <0.5 μm. The matrix K-feldspar is usually orthoclase and is featureless. Vein perthite sheets are irregular and can be 100 μm thick. The veins are turbid. The K-feldspar in the veins is usually microcline, and combined Albite-Pericline twinning may be visible. In Shap the Ab-rich phase in veins is oligoclase. Pure replacive albite corresponds with turbid regions forming along, and extending from, film lamellae, at various scales. (**b**) Features visible in a (001) foil using TEM. [1] The periodicity (λ) of thicker film albite lamellae is typically near 1 μm, but thinner, shorter lamellae are often present. Platelets are only a few nanometers thick and tens of nanometers in length. Albite and Pericline twins are visible in albite lamellae. In extended lamellae the periodicity of Albite twins is typically ~20 nm but varies in proportion to the thickness of the lamellae (shown qualitatively). In Shap, Pericline twins in albite are sub-parallel to (001) (see **c**), and the albite appears untwinned viewed on (001). The orthoclase has visible tweed. Nanotunnels (formed by dissolution along misfit dislocations), and pull-aparts, develop on thicker film lamellae; their spacing varies with lamellar thickness. Both features can be imaged on HF etched cleavage surfaces using SEM. [2] Vein perthite is composed of parallel oligoclase and microcline subgrains, the latter concentrated near the edges of veins. Micropores form at subgrain junctions, causing optical turbidity. [3] Late replacive albite begins to form as 10 nm thick peg-shaped subgrains nucleated on nanotunnels, which grow and merge to form albite regions on >10 μm scales. Subgrains often have the {110} Adularia habit. Albite twin periodicities are >20 nm and micropores are abundant. (**c**) Orientation of features visible on (010). The drawing is at TEM scale; film lamellae are usually <1 μm thick. Albite film lamellae and Pericline twins in microcline are usually visible using LM but Pericline twins in albite lamellae require TEM. Nanotunnels and pull-aparts require TEM, or SEM of HF-etched surfaces. The composition plane of Pericline twins (the so-called rhombic section) in alkali feldspars rotates about the *b*-axis depending on composition and structural state [broken lines, from Smith and Brown (1988), Fig. 18.8]. In Shap the Pericline twins in film perthite lamellae are close to the high albite position, although they are composed of low albite (see Fitz Gerald et al. 2006). The Or-rich feldspar containing film lamellae is tweed orthoclase, with microcline occurring only in veins (**b**, [2]) but many K-feldspars from granites are predominantly microcline with tartan twinning on LM scales. In this case film albite lamellae in ($\bar{6}$01) are sub-parallel to Pericline twins in microcline and may be hard to see using LM. Difference in relief can show the presence of film lamellae. Far from crystal surfaces, nanotunnels are <10 nm in diameter, but near surfaces they are enlarged by weathering to >1 μm (Lee and Parsons 1995; Lee et al. 1998). Pull-aparts are in (001) and therefore make a small angle with Pericline twins.

(1932), by replacement, in "deuteric" (i.e., of magmatic origin) or externally derived "hydrothermal" fluids, and also from "cold waters under vein conditions." The controlling factor is the presence of a miscibility gap, defined by a ternary solvus surface in the system Ab-Or-An, often simplified to alkali feldspar solvus for compositions near the Ab-Or join. The term exsolution (or unmixing) is sometimes restricted to intergrowths produced by a continuous process from a homogeneous parent, but the ternary solvus defines phase compositions even in intergrowths formed by replacement, so the term is appropriate for all perthitic intergrowths. The mechanisms of formation of complex perthitic intergrowths have been the subject of numerous review articles: Smith (1974, Chap.19), Parsons and Brown (1984, 1991), Smith and Brown (1988, Ch. 19); Brown and Parsons (1989, 1993, 1994), Parsons and Lee (2005).

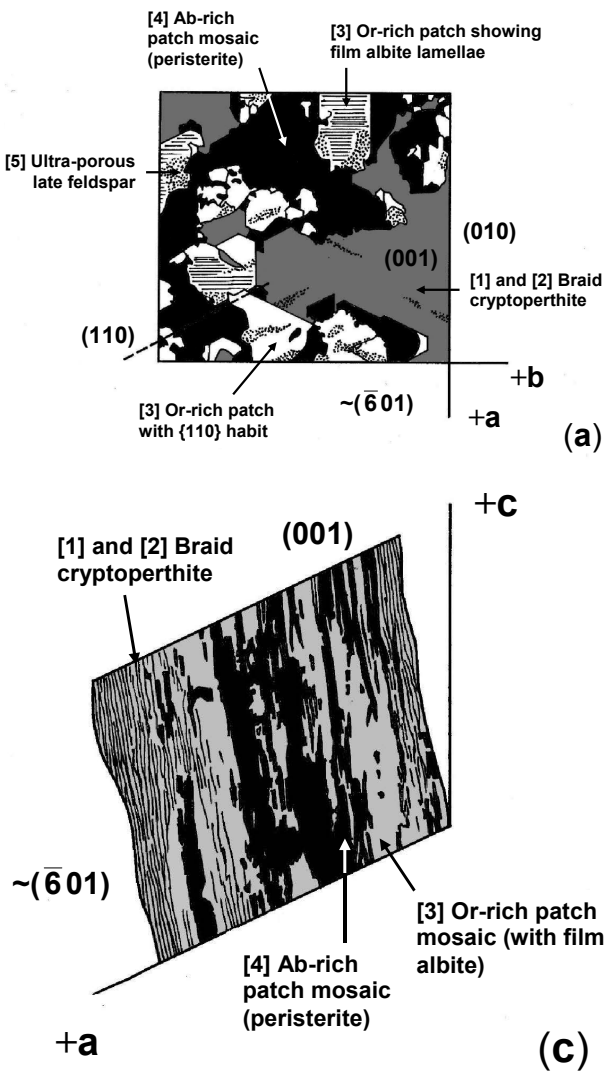

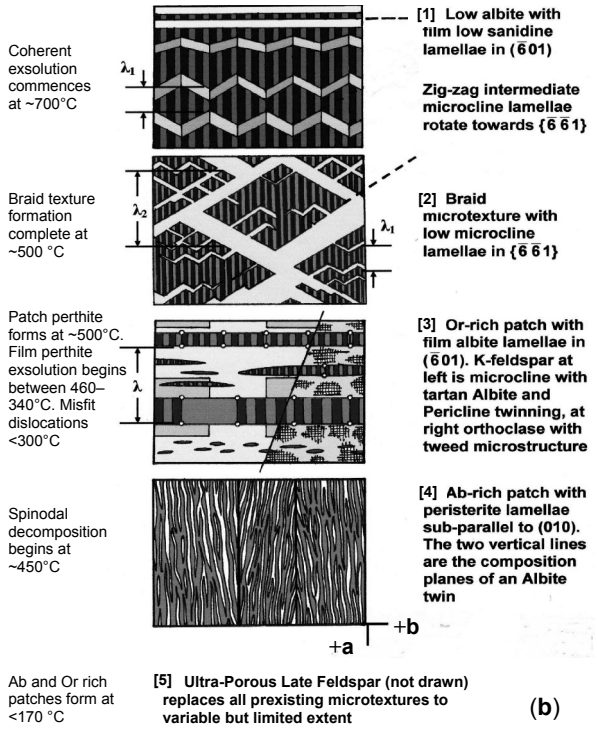

FIGURE 2. Cartoons illustrating microtextures in alkali feldspars from Klokken syenites. Similar microtextures occur in hypersolvus granites except that replacive intergrowths often have a vein morphology. See text for supporting micrographs. Orientations and grayscale relationships are as in Figure 1. Angular relationships are drawn accurately. Items numbered in square brackets are the same feature in each drawing. (**a**) Features visible on (001) using BSE imaging in an SEM. The field is ~500 μm across. Numbers in square brackets correspond with features shown at high magnification in **b**. Medium-gray areas ([1] and [2]) are glass-clear using LM and are fully coherent braid cryptoperthite, which is unresolved in this example at this scale. Coarse braid intergrowths can be resolved using BSE, and using LM with care. The braid microtexture is structurally continuous except where it has been replaced by patch perthite composed of subgrains and subgrain mosaics of Or-rich (white, [3]) and Ab-rich feldspar (black, [4]). In Klokken this Or-rich phase is usually microcline, with twinning visible in LM, rarely orthoclase. Patch perthite regions are turbid in LM. Many replacive subgrains have the distinctive {110} Adularia habit. Or-rich subgrains contain film albite lamellae [3] that are just visible at this magnification, and visible using LM with care. Ab-rich subgrains [4] are a peristeritic intergrowth, below SEM resolution. Ultraporous late feldspar (UPLF) [5], shown by dotted regions, replaces all preceding intergrowths but is most common in patch perthite regions where it leads to extreme turbidity in LM. (**b**) Features visible on (001) using TEM. [1] and [2]. In Klokken, fully coherent microtextures evolve geometrically and coarsen systematically with respect to the roof of the intrusion. Near the roof, straight film lamellae [1] have average λ of ~55 nm. Downward, coarsening and framework ordering leads to zigzag intergrowths which mature into braid textures [2] with interfaces in $\{\bar{6}\bar{6}1\}$, with a primary periodicity (λ_1) of ~30–400 nm. There is a coarser secondary periodicity (the broad microcline bands in [2]), with λ_2 up >600 nm, that can be seen using LM. [3] Straight film lamellae develop in $(\bar{6}01)$ in replacive Or-rich subgrains, which have bulk compositions in the range Ab_{10} to Ab_{20}. The film lamellae have mean λ of ~1 μm and can be seen, with care, using LM. These intergrowths have much in common with the film intergrowths in the Shap feldspars (Fig. 1b) with similar periodic nanotunnels and pull-aparts visible using TEM or on HF etched cleavage surfaces. The Or-rich phase in the Or-rich patches is usually Albite and Pericline twinned microcline, less commonly tweed orthoclase (tweed texture visible only using TEM). [4] A peristerite intergrowth has been found using TEM in Ab-rich patches (bulk composition ~$Ab_{91}An_8Or_1$) in one sample. Mean λ is 17 nm. [5] No attempt has been made to draw UPLF; see Parsons et al. (2013) for TEM micrographs. It is composed of near-end-member Ab- and Or-rich regions which replace all preexisting microtextures, distinguished by extremely irregular internal diffraction contrast. Where braid perthite and Or-rich patches with film perthite are replaced, ghost-like relics persist in the UPLF as "textural pseudomorphs," but where Ab-rich patches (including peristerite) are replaced a discrete subgrain microtexture develops. (**c**) Features visible on (010) using BSE. In this orientation braid perthite ([1] and [2]) appears as sinuous pillars at sub-micrometer scale and patch perthite ([3] and [4]) has a vein morphology at scales of up to hundreds of micrometers.

It is important to use terminology rigorously when describing perthitic intergrowths. We advocate that component is best restricted to its thermodynamic sense: $NaAlSi_3O_8$ (abbreviated to Ab), $KAlSi_3O_8$ (Or), and $CaAl_2Si_2O_8$ (An). A fourth component, $BaAl_2Si_2O_8$, celsian, (Cs), may sometimes exceed An. A guide to terminology, based mainly on the recommendations of Smith and Brown (1988), is provided by Parsons (2010). Alling (1921) correctly emphasized that "perthite is an intergrowth of two or more solid solutions and not an intergrowth of the simple components microcline … and acid plagioclase." At stable equilibrium the three main components are distributed between a maximum of two feldspar phases so that the chemical potential of each component is the same in both phases. This relationship forms the basis of modern two-feldspar geothermometry (Brown and Parsons 1981, 1985). Details of current thermometers are given below in the section on thermochronology. Because the thermometers depend only on the partitioning of feldspar components between feldspar phases they are independent of other phases and components in the rock. They are sensitive to P, raising exsolution T in binary Ab-Or feldspars by ~22 °C/100 MPa (Hovis et al. 1991) but not to P_{H_2O}, because water does not dissolve significantly in feldspar and therefore does not affect the chemical potentials of the components. Two-feldspar geothermometers can be applied to feldspar pairs growing on the ternary feldspar solvus, or to phases coexisting in equilibrium in perthitic intergrowths. Many perthitic intergrowths contain more than the two phases dictated by the phase rule. Such complex microtextures reflect phase behavior rather than phase equilibria (Brown and Parsons 1989).

Figures 1 and 2 are cartoons designed to provide a framework for this review, and to illustrate the appearance of microtextures viewed from the most convenient and informative directions, which are normal to the perfect cleavages (001) (Figs. 1a–1b and 2a–2b) and (010) (Figs. 1c and 2c). Although some phases in the intergrowths have triclinic symmetry ($C\bar{1}$), repeated twinning means that the macroscopic symmetry of almost all alkali feldspar (and plagioclase) crystals or cleavage fragments is monoclinic ($C2/m$). Miller symbols and axial directions in the text below, and in Figures 1 and 2, relate, unless otherwise stated, to the average monoclinic morphology.

Figure 1 is based mainly on micrographs of alkali feldspars from Shap, bulk composition near $Ab_{29}Or_{70}An_1$, in Lee et al. (1995), Walker et al. (1995), Lee and Parsons (1997b), Fitz Gerald et al. (2006), and Parsons et al. (2010). Observations on feldspars from other granites by ourselves and coworkers, and in the literature, suggest that the Shap examples are reasonably representative of alkali feldspars from sub-solvus granitoids, although many have lower bulk Or, suggesting lower crystal growth T. Figure 2 illustrates microtextures in alkali feldspars from Klokken which have bulk compositions near ($Ab_{60}Or_{40}$) $An_{1–5}$ and is based mainly on micrographs in Parsons (1978, 1980), Brown et al. (1983), Brown and Parsons (1984a, 1984b, 1988), Parsons and Lee (2009), Parsons and Fitz Gerald (2011), and Parsons et al. (2013). The order of the formation of the microtextures deduced from cross-cutting relationships corresponds with falling T inferred from ternary solvus relationships (Lee and Parsons 1997b; Parsons et al. 2013). The T of various events is given on the left of Figures 1b and 2b. This aspect of the intergrowths is discussed further in a section on thermochronology below.

Six interacting factors underlie the microtextural diversity:

(1) Exsolution of an initially homogeneous ternary solid solution leads to perthitic intergrowths of Or- and Ab-rich feldspar phases. Perthitic intergrowths below the resolution of LM are called cryptoperthites, those visible using LM are microperthites, and those visible in hand-specimen are macroperthites. The word "perthite" is often used generically but perthites sensu stricto have Or-rich bulk compositions (like Shap), with Ab-rich lamellae in an Or-rich matrix, those with approximately equal Ab:Or are mesoperthites and those in which Or-rich lamellae occur in an Ab-rich matrix are antiperthites. Note that these terms are purely compositional [see Smith and Brown (1988, Fig. 1.6b) and Parsons (2010, Fig. 1.3) for a simplification]. The word "mesoperthite" is sometimes used specifically for the coarse, lenticular or sinuous intergrowths characteristic of granulites, but this is too restrictive. Crypto-antiperthites, crypto-mesoperthites, and crypto-perthites all occur in Klokken (Parsons and Brown 1983; Brown and Parsons 1988; Parsons et al. 2013). Note that the word "perthite" applies to the totality of the intergrowth of Ab- and Or-rich phases, not, as it is sometimes used, only for the lamellae of Ab-rich feldspar in an intergrowth.

(2) Phase boundaries may be fully coherent (sharing a continuous Si-Al-O framework), leading to elastic coherency strain to accommodate differences in cell dimensions, semi-coherent (with periodic misfit dislocations that lower total coherency strain energy, Figs. 1b, 1c, and 2b [3]) and incoherent, composed of parallel or sub-parallel discrete subgrains (Figs. 1b and 2a) within the outline of a single feldspar crystal. Coherent intergrowths form by volume diffusion and their morphology and related repeated (or polysynthetic) twinning, which is also coherent, are functions of bulk composition and thermal history (Brown and Parsons 1988, Fig. 9), and are primarily governed by minimization of coherency strain energy (Willaime and Brown 1974). Incoherent intergrowths are usually developed by replacement reactions involving a post magmatic (deuteric) or externally derived (hydrothermal) fluid.

(3) Color and transparency are extremely important features of alkali feldspars, directly related to the underlying microtextures. Feldspars that have escaped reactions with aqueous fluids are clear (pristine) and colorless in LM. This is not uncommon in phenocrysts from volcanic rocks and there are some celebrated examples of "gem-quality" crystals of great perfection from pegmatites (see Parsons and Lee 2005, for a review). Completely or largely pristine alkali feldspar is very rare in plutonic rocks, is black or dark bottle-green in the mass, and sometimes shows iridescence caused by Bragg diffraction of light by exsolution microtextures. The best-known example is the syenite variety, larvikite, quarried near Oslo as an architectural stone. The Klokken syenite is a larvikite, with feldspars that are sometimes iridescent. Other examples of pristine feldspar come from some rapakivi granites (Harrison et al. 1990), charnockites (Fitz Gerald et al. 2006), and granulite-facies metamorphic rocks (Cayzer 2002).

The overwhelming majority of plutonic alkali feldspars are partly or completely turbid in thin section, caused by high concentrations of micropores (Worden et al. 1990; Walker et al. 1995). Many are, or were, fluid filled (Johnson and Rossman 2004) and most, although not all, are associated with replace-

ment of pristine microtextures with a mosaic of Ab- and Or-rich subgrains, with micropores at their junctions. Mineral particles in the pores impart the color of many feldspars, predominantly ilmeno-magnetite in white or gray crystals (Worden et al. 1990), hematite in pink and red crystals (Putnis et al. 2007).

(4) During cooling, Ab-rich feldspars pass through an instantaneous, reversible $C2/m$–$C\bar{1}$ shearing phase transition (also called a displacive transition) that involves significant changes only in the α and γ cell angles and does not involve breaking of bonds. It is discussed at length by Smith and Brown (1988, Ch. 7). The transition T varies with Ab:Or but is also sensitive to An and Si-Al order. In disordered albite the symmetry change is at ~1000 °C, and at room T in metastable feldspars below the solvus it is at ~$Ab_{60}Or_{40}$. It intersects the equilibrium order solvus at ~700 °C and $Ab_{80}Or_{20}$. The symmetry change leads to the development of relatively regular, fine-scale twinning on the Albite and Pericline laws (note use of capitals) that maintains the macroscopic $C2/m$ symmetry of the parent crystal. Twinning formed in this way is characteristic of anorthoclase crystals in volcanic rocks, but it is common at the TEM scale in the Ab-rich phase of perthitic alkali feldspars. The composition plane of Albite twins is (010) in all feldspars, and is thus parallel to the perfect (010) cleavage. The composition plane of Pericline twins always contains the **b** axis, and is therefore normal to (010) in monoclinic feldspars, or at a small angle from the normal in triclinic feldspars, up to 94.3°, in low albite. However, it rotates about **b** depending on chemical composition and degree of framework order, and lies in a non-integral (sometimes called "irrational") plane called the rhombic section. This plane is not, in general, parallel to any cleavage (e.g., Fig. 1c).

(5) Unless they cool very rapidly, both Ab- and Or-rich alkali feldspars undergo a relatively slow diffusive phase transition involving framework Si-Al ordering. In Ab-rich feldspars (triclinic, $C\bar{1}$) this leads to a continuous change in cell dimensions and angles from high- to low-albite, but no change of symmetry. Ordering in Or-rich feldspars leads to a transition from $C2/m$ sanidine to $C\bar{1}$ microcline. The complexities of ordering and the nomenclature of K-feldspars are discussed by Smith (1974, Ch. 9), Smith and Brown (1988, Ch. 9), and Brown and Parsons (1989). A skeletal summary is given here to introduce terminology. There are four equivalent tetrahedral sites in feldspars, called $T_1(0)$, $T_1(m)$, $T_2(0)$, $T_2(m)$. In monoclinic feldspars the paired T_1 and T_2 sites are respectively related by mirror symmetry and are indistinguishable. In fully disordered alkali feldspars the T sites are occupied at random by Si and Al atoms in the ratio 3:1, but in fully ordered feldspars all Al is in $T_1(0)$. The ordering behavior of Na and K feldspars differs. Disordered albite is monoclinic (monalbite) above the shearing transformation at ~1000 °C. Below this T the stable phase is triclinic high albite. The identity of the $T_1(0)$ site is defined at the beginning of ordering by the shearing transformation and the resulting triclinic symmetry. With decreasing T Al diffuses into $T_1(0)$ from $T_1(m)$ and the T_2 sites, a process called convergent ordering, and there is an equilibrium degree of order which increases with falling T. There is a continuous transition to ordered low albite but most ordering occurs in the range 720–650 °C (at low P), an interval over which intermediate albite is stable. Ordering in albite is rapid and in the majority of perthitic feldspars the Ab-rich phase is ordered low albite.

In Or-rich feldspars disordered monoclinic high sanidine is stable at >900 °C. Ordering begins by movement of Al from T_2 to both T_1 sites, and if Al is distributed randomly between T_1 sites monoclinic symmetry is maintained. This is called non-convergent ordering. Sanidine orders continuously with decreasing T giving partly ordered $C2/m$ low sanidine, with most Al in T_1 sites, at ~ 700 °C, the increasing order being marked mainly by change in optical orientation and optic axial angle, $2V$ (Su et al. 1986),

Once most Al is in T_1 further ordering requires Al to concentrate in one or other of the undifferentiated T_1 sites. In albite, $T_1(0)$ is defined by the shearing transformation, but in the monoclinic framework of sanidine Al has two "choices," which can be thought of as "left" and "right" orientations relative to the mirror plane. A TEM-scale "tweed" microstructure of triclinic domains on a scale of a few unit cells develops, in the same orientation as Albite and Pericline twins. Tweed is the defining characteristic of orthoclase. Orthoclase is monoclinic in LM and PXRD but gives diffraction spots in SXRD and SAED that are streaked, because of short-range ordering, in directions corresponding with Albite and Pericline twinning. Orthoclase is defined using LM by $2V \geq 50°$ (Su et al. 1986).

Orthoclase is not fully ordered but has ~80% of its Al distributed randomly between $T_1(0)$ and $T_1(m)$ sites; ideal, fully ordered low microcline has all its Al in the T_10 site. Further ordering involves a $C2/m$-$C\bar{1}$ symmetry change and low microcline has a the maximum departure of the α and γ cell angles from 90°, the obliquity of the feldspar. The terms maximum microcline and triclinicity were used in early work. Early terminology is discussed by Smith (1974, Ch. 7). Mechanisms of the orthoclase-microcline transition are discussed below. Intermediate microcline, with less than maximum obliquity, is common in Nature but its status as a stable phase is controversial [compare Brown and Parsons (1989) with Carpenter and Salje (1994)]. During this symmetry change, repeated, often irregular, "cross-hatched" or "tartan" (Smith and Brown 1988, p. 541) Albite and Pericline twins usually develop on a range of scales. This again maintains the macroscopic $C2/m$ symmetry of the parent crystal.

Adularia is a frequently encountered but extremely poorly defined term. It is a K-feldspar defined by its habit, with strong development of {110} faces and weak development of {010}, and by its low-T origin. It occurs in Alpine-type veins, some metasomatic rocks and as authigenic overgrowths in sedimentary rocks. It can be monoclinic or triclinic, or mixtures thereof, and often has anomalous optical and XRD properties. It is a common habit for subgrains in replacement perthites (Figs. 1b and 2a) although these demonstrably form at T as high as 500° (Fig. 2a). The equivalent Na-feldspar is pericline.

(6) Using TEM a peristerite intergrowth has recently been discovered in the Ab-rich phase of a coarse mesoperthite from Klokken (Parsons and Fitz Gerald 2011; Parsons et al. 2013). Peristerites are nanometer-scale intergrowths of albite and oligoclase that form by exsolution at a coherent solvus that is conditional on Si-Al ordering (Carpenter 1981). This is the first such intergrowth found in a perthitic crystal using TEM, but on compositional grounds they may well be common. A 1 μm scale two-plagioclase intergrowth found using BSE SEM imaging and

high-resolution EPMA, in the Ab-rich phase of a mesoperthitic patch perthite from a granulite facies rock (Abart et al. 2009b), may be related to peristerite, but this requires crystallographic confirmation.

Early LM work led to the recognition of many varieties of perthite (Smith and Brown 1988, pp. 577–604). We here use simplified terminology that covers the majority. The terms film, vein and patch perthite were adopted by Andersen (1928). In recent work (e.g., Brown et al. 1983 and many subsequent papers) the term braid perthite has come to be used for mesoperthites with coherent interfaces near $\{\bar{6}\,\bar{6}1\}$ (Fig. 2b), in which albite forms columns with a diamond-shaped cross section (Figs. 2b and 2c). Feldspars of this type were first described by Brøgger (1890) in larvikitic syenites from the Oslo alkaline province, similar to those in Klokken. However, the first use of the term was by Goldich and Kinser (1939), for coarser incoherent intergrowths with interfaces in {110}, considered to be formed, at least in part, by replacement. In these intergrowths the compositional relationships are reversed compared with Figure 2b. The "diamonds" in Goldich and Kinser's type material are K-feldspar and the films albite. Examples are given by Smith and Brown (1988, Fig. 19.23)

Intergrowths fall into two classes, respectively formed by diffusion and by replacement. These are described in detail in the next two sections. Both processes are strongly coupled with Si-Al order-disorder in the framework and to associated twinning, which we describe in a third section. In each section we first describe crystallographic and phase relationships and then in a sub-section review geological applications ranging from post-magmatic processes to weathering and diagenesis.

Coherent and semi-coherent intergrowths formed by diffusion

Intergrowths that develop by diffusion are crystallographically regular and develop in well-defined orientations (see below) on scales below a few tens of micrometers. They form primarily by $Na^{1+} \leftrightarrow K^{1+}$ interdiffusion in a Si-Al-O tetrahedral framework that remains coherent or becomes semicoherent. If Ca^{2+} is present most of it enters the Na-rich phase, because of the similar ionic radii of Ca^{2+} and Na^{1+}, but it has to be accompanied by Al^{3+} replacing Si^{4+} to maintain charge neutrality. Because of its large ionic radius Ba^{2+} goes into the Or-rich phase. Small amounts of Ca increase exsolution *T* considerably (reviewed by Parsons et al. 2009), but probably slow exsolution rates because of the need to move coupled Al^{3+} ions in the framework.

Intergrowths formed by diffusion are often described as "strain controlled." Because of the different ionic radii of Na^{1+} and K^{1+} coherent elastic strain arises at the interface between embryonic Na- and K-rich regions. As embryos coarsen their interfaces develop along planes of minimum coherency strain energy (Willaime and Brown 1974; Parsons and Brown 1991). Depending on crystal bulk composition the interfaces between coexisting phases may remain fully coherent or become semicoherent, with periodic misfit dislocations (Aberdam 1965; Brown and Parsons 1984b, 1988; Waldron et al. 1994; Fitz Gerald et al. 2006).

Exsolution can occur by spinodal decomposition [Cahn (1968); for a review of experimental work on feldspars see Parsons and Brown (1991)], which is the dominant process for bulk compositions near the solvus critical composition. In this process a low-amplitude compositional wave develops in which one wavelength is amplified defining an initial periodicity, which coarsens with time (see below). On the flanks of the solvus coherent nucleation is the more probable exsolution mechanism. During nucleation the matrix is locally depleted in the component that is contributing to the growing nucleus. Nucleation may be homogeneous (spontaneous and unrelated to preexisting structural features) or heterogeneous (related to defects or inclusions).

Whatever the mechanism, when compositional equilibrium is reached, phase compositions define a metastable coherent solvus, which plots inside the stable equilibrium or strain-free solvus. Parsons et al. (2010, Fig. 1) give a compilation of experimentally determined solvus curves and their sources. Depending on cooling rate, a feldspar may pass through the coherent solvus without exsolving, but it will unmix rapidly at the coherent spinodal, which lies inside the coherent solvus except at the critical temperature where the curves are in contact. In the real world, phase compositions are governed by ternary phase equilibria and all these curves are represented by tunnel-shaped ternary surfaces. Carmichael (1974, Fig. 5-1) provided the first correct general depiction of the ternary feldspar system but because of difficulties in obtaining equilibrium (see e.g., Elkins and Grove 1990) it has still not been fully determined by direct synthesis. Very low concentrations of An increase exsolution *T* in alkali feldspars considerably and there are uncertainties in the role of An at low *T*, discussed by Parsons et al. (2009).

The periodicity, orientation, morphology and twinning of coherent exsolution lamellae are functions of bulk composition and cooling rate (Brown and Parsons 1988, Fig. 9). Symmetry changes during framework Si-Al ordering lead to development of periodic twinning (Figs. 1 and 2) and in some cases rotation of interfaces into new orientations (Fig. 2). In crystals with Or-rich bulk compositions, common in "sub-solvus" granitic rocks (Fig. 1), the coherent Ab-rich phase forms extended lenses (usually called film lamellae, and often nearly parallel-sided), in a plane between $(\bar{8}01)$ and $(\bar{6}01)$ (the so-called "Murchison plane" of easy fracture), that is non-integral because of coherency strain. Comparatively coarse lenticular exsolution lamellae in mesoperthites from the granulite facies, with a relatively low aspect ratio, were called "spindles" by Evangelakakis et al. (1993) and Abart et al. (2009b) but a spindle has a circular section at right angles to its long axis. Evangelakakis et al. state that their spindles were more elongated in sections parallel to (010) than in (001) so they should be regarded as a variety of film perthite. Abart et al. do not give the orientation of any of their numerous micrographs, so the three dimensional form of their interesting microtextures cannot be assessed. Our experience is that "spindles" are often extended in $(\bar{6}01)$, sub-parallel to **c*** (Brown and Parsons 1984b, 1988, 1993; Lee and Parsons 1997b; Lee et al. 1995; Parsons and Fitz Gerald 2011; Parsons et al. 2010, 2013).

The Or-rich phase in film perthites is either sanidine or usually, in a plutonic setting, orthoclase, although film lamellae also occur in microcline. Misfit dislocations form on lamellar interfaces as lenses coarsen (Fig. 1b), the structure stiffens with falling *T*, and coherency strains become unsustainable. These de-

fects probably account for the fracture property of the Murchison plane. Unless they intersect a crystal surface the dislocations form very flat lenticular loops encircling lens-shaped lamellae, both in the **a**–**c** plane and parallel to **b**. They form both in perthites ss. (Lee et al. 1995) and antiperthites (Brown and Parsons 1984b) and are important in providing pathways for fluids to enter crystals during replacement reactions (Lee and Parsons 1997a). They are often enlarged by dissolution to produce orthogonal networks of "nanotunnels" (Fig. 1b), each a few nanometers in diameter (Fitz Gerald et al. 2006). When nanotunnel loops intersect, the opposite sides are often connected by minute cleavage cracks [parallel to (001) or (010)] that we called "pull-aparts" (Fig. 1b). The "line defects" reported in a granulite facies feldspar by Abart et al. (2009b, Figs. 7a and 7b) seem to be pull-aparts (compare with Fig. 3 in Fitz Gerald et al. 2006). Very small, fully coherent lenticular exsolution lamellae are common and often called "platelets" (Fig. 1b). These frequently occur in "stranded diffusion profiles" between longer and thicker lamellae (Lee et al. 1995, Figs. 10 and 15; Parsons et al. 2013, Fig. 8c).

Applications of intergrowths formed by diffusion

The bulk composition of coherent and semicoherent microtextures can be used to estimate the minimum T at which the feldspar crystallized, which must be above the ternary strain-free solvus, and the T at which the feldspar cooled through the coherent solvus. Provided coherency is maintained in the periodic intergrowths we can be confident that the bulk composition has been unchanged since the beginning of coherent exsolution. Solvus curves are discussed below in a section on Thermochronology, and methods of estimating bulk composition are described under Recommended Routine Methods in the EPMA section. These relationships can be applied to microtextures developed in entire crystals, or relics of such microtextures remaining in more complex crystals. It is reasonable to assume that prior to deuteric reactions in Klokken entire crystals were initially braid perthite (Fig. 2b [1,2]) or in Shap that entire crystals were once entirely film perthite (Figs. 1a and 1b [1]). The same reasoning can be applied to sub-regions of crystals such as the film lamellae in Or-rich patches in Klokken patch perthite (Fig. 2b [3]).

Coarsening rates of film microperthite. Simple planar lamellar microtextures produced by volume diffusion can be used with some confidence in feldspars with low An to estimate cooling rates of volcanic and minor intrusive rocks [(reviewed by Yund (1984) and by Parsons and Brown (1991)]. The method relies on experimentally determined lamellar coarsening rates determined by measuring the periodicity (the repeat distance, λ, Figs. 1 and 2) of intergrowths formed by spinodal decomposition in sections normal to the lamellae. It must be stressed that these methods can be applied only to regular, coherent or semicoherent film lamellae produced by diffusion. These have smooth surfaces and regular orientations near ($\bar{6}$01). They should not be applied to replacive vein lamellae, which have irregular surfaces and are composed of subgrains, even when they are sub-periodic (see next section). The mechanism of coherent coarsening is discussed by Brady (1987). Lamellae in sub-planar intergrowths have "wedge-shaped ends," which retreat on thin lamellae as adjacent lamellae coarsen. Coarsening is described by the expression $\lambda_t^2 = \lambda_0^2 + k_T t$, where k_T is a T-dependent rate constant and λ_0 the initial wavelength of spinodal decomposition, in the range 9–20 nm, increasing with T.

For plutonic bodies calculation of cooling rates from coherent film lamellae is uncertain because of long extrapolations in t from the range of diffusion experiments and because of coupling between exsolution and Si-Al ordering, and associated twinning. Parsons and Brown (1991) suggested that the relationship above should be limited to cooling times $<10^3$ years. In Klokken, albite film lamellae developed in Or-rich patches subsequent to a phase of isochemical replacement below ~450 °C (Figs. 2a and 2b [3]). These have λ ~1 μm (Parsons and Lee 2009, Fig. 7; Parsons et al. 2013, Figs. 4–8). λ does not vary with position in the intrusion, although the coherent braid perthites that preceded the development of the film perthites (Fig. 2b, [1] and [2] and see below) show a strong linear relationship between $\log_{10}\lambda$ and stratigraphic height. This is probably because by the time film exsolution began, at <450 °C, thermal gradients were low. The film lamellae formed by coherent nucleation, sometimes demonstrably heterogeneous. Parsons and Fitz Gerald (2011) used the Einstein approximation $x^2 = Dt$ to calculate λ_T, where x is the mean diffusion length, λ/2, and the diffusion coefficient, D, was calculated from the experimental coarsening study of Yund and Davidson (1978). We found good order-of-magnitude agreement between calculated and observed λ, and a cooling trajectory for Klokken calculated by Brown and Parsons (1984a), based only on conductive heat loss, which suggested that exsolution and coarsening of film perthite occurred 10^4–10^5 years after crystallization.

Chemical zoning developed during crystal growth can lead to variation in λ of film perthites [Lee and Parsons (1997b), for Shap; Abart et al. (2009a), in an Austrian granite; Nakano (1998), in a Japanese quartz syenite]. Zones with smaller λ correspond with slightly higher An (and also, in Shap, Ba feldspar, Cs). An partitions into the Ab-rich phase and slows coarsening rates because of coupling of Ca^{2+} with framework Al^{3+}. It also raises the T of the beginning of exsolution because of the domed shape of the coherent ternary solvus, but this does not seem to compensate for the slower kinetics. Abart et al. show that magmatic zoning can affect not only the coarseness of exsolution textures but also the mechanism of exsolution. The microtextures in the Austrian granite are very different to Shap, probably because Abart et al.'s sample has higher bulk An. However, it is difficult to compare the two studies because the latter authors do not give the orientation of their micrographs. A similar comment applies to the paper by Tajčmanová et al. (2012), in which the Feret diameter (the longest diameter) of exsolution lamellae is considered without illustration or discussion of their possible three-dimensional shape. We cannot stress too strongly the need to give the orientation of micrographs of intergrowths that in general look very different depending on the viewing direction (compare the sections in Fig. 2).

Film lamellae are often extended, flat lenses in three dimensions, and what appears to be a short, thin lamella may in three dimensions be a marginal section of a much longer and thicker lamella. In our view the best way to obtain λ, and hence define the mean diffusion length, is by measuring the spacing on equivalent surfaces of all lamellae, large and small, (but not including platelets in stranded diffusion profiles, Figs. 1b [1] and 2b [3]), on a predetermined line of traverse at 90° to the lamellae. This was the method adopted by Brown et al. (1983) (present Fig. 2b). Ideally,

the lamellae should be at 90° to the surface of the section but film lamellae in $(\bar{6}01)$, or the diamond-section $\{\bar{6}\bar{6}1\}$ columns of albite in braid intergrowths (Fig. 2b), are almost normal to (001) (Fig. 1c) so measurement in (001) sections leads to an overestimate of periodicity of only 4 to 5%, depending on the exact value of *h* and cell parameters. Note that the lamellar interfaces are non-integral planes.

In our experience film lamellae in feldspars from granitic rocks usually have mean λ mostly at the lower end of a 1–5 μm range, in various geological settings and likely thermal histories. Examples from granitic rocks are given by Walker (1991), Waldron et al. (1994), Lee et al. (1995), Lee and Parsons (1997a, 1997b, 1998), Parsons and Lee (2005), and Flude et al. (2012). The samples studied by Walker come mostly from intrusions in the Scottish Highlands of a range of sizes emplaced during the late Caledonian orogenesis. Shap is a small (3 × 2 km) relatively high-level pluton, and Flude et al. (2012) studied feldspars from the relatively large Dartmoor batholith in SW England. Parsons and Lee (2005, Fig. 11a) illustrate semicoherent film perthite in the very rapidly exhumed Tato granite from Nanga Parbat in the Himalaya, which has an intrusion age of only 1 Ma (Zeitler et al. 1993). All these diverse intrusions have film lamellae with λ ~1–5 μm.

In the very different setting of the granulite facies, Abart et al. (2009b) and Tajčmanová et al. (2012) also found film albite lamellae in Or-rich patches ascribed to an earlier phase of deuteric coarsening that have micrometer-scale λ. Many alkali feldspars from granulites appear to have at least a two-stage exsolution history, in which a late phase of exsolution leads to film lamellae on scales of a few micrometers [Evangelekakis et al. (1993); Waldron et al. (1993); Cayzer (2002), examples are given in Parsons et al. (2005), Fig. 19]. Taken together, the data on film perthites in granites, the late post-coarsening perthites from Klokken and various granulites, suggest that film perthite periodicities in plutonic rocks are not a useful guide to cooling rates. Studies that led Yuguchi and Nishiyama (2007) and Yuguchi et al. (2011a) to a different conclusion are reviewed in a later Discussion section.

The coarsest film mesoperthites come from granulite-facies rocks, and have λ in excess of 10 μm, broadly consistent with long periods of annealing at elevated *T* (Parsons et al. 2005; Cayzer 2002; Abart et al. 2009b; Tajčmanová et al. 2012). Exsolution textures in these rocks are generally coherent or semicoherent. Nanotunnels have been found even in these "dry" rocks (Fitz Gerald et al. 2006) and retrogression in granulite feldspars can be indicated by replacive subgrains (Waldron et al. 1993).

Coarsening rates of braid microperthite. In the mesoperthitic feldspars found in syenites (bulk ~$Ab_{60}Or_{40}$), coherent coupling between the initially monoclinic Or-rich phase and volumetrically dominant triclinic Ab-rich phase leads to microcline formation (Lorimer and Champness 1973; Brown and Parsons 1984a, 1988; Waldron and Parsons 1992). The morphology of the microtextures and their evolution are dominated by minimization of coherency strain energy (Willaime and Brown 1974). Exsolution begins at higher *T* (>700 °C) than in granites. Planar films in $(\bar{6}01)$ form initially (Fig. 2b) and Albite twins develop when the initially monoclinic Ab-rich phase intersects the shearing transformation. Interfaces then rotate into $\{\bar{6}\bar{6}1\}$ as Si-Al ordering occurs, leading to zigzag or braid intergrowths (see section on twinning, below). Dislocations do not form because coherency strains are minimized by interface rotation and by twinning. TEM work has shown that in both Klokken (Brown et al. 1983) and the Coldwell intrusion (Waldron and Parsons 1992) λ increases with distance from intrusive contacts but the largest primary λ are only ~400 nm, considerably smaller than many film perthites. In the Klokken intrusion, which has a well-constrained three-dimensional shape, λ increases regularly in a log-linear fashion with distance from the roof, over a 550 m vertical section, from ~50 to ~300 nm (Brown et al. 1983). In the larger Coldwell complex, λ increases slightly inward with respect to the wall of the intrusion, from ~50 to 90 nm, but the shape of the intrusion is less well known than Klokken. Calculated cooling curves for Klokken (Brown and Parsons 1984a) suggest that braid perthite formed between 10^3 and 10^4 years after crystal growth. Exsolution in the braid perthites began at higher *T* (>700 °C) than in film perthites in Or-rich patches (<500 °C), which have micrometer-scales, but the rate of coarsening of braid is coupled with ordering and associated twinning through coherency, and this limits the final periodicity. There is no way at present to determine coarsening rates experimentally or theoretically in these coupled intergrowths. Film perthite exsolution (see above) begins when the feldspar is either orthoclase, with a high degree of order, or fully ordered low microcline, and there is no rate-limiting coupling.

Coherent and semi-coherent microtextures maintain permanent elastic strain which can be released by dissolution and deformation (next section). Norberg et al. (2011) made the very interesting discovery that during experimental replacive albitization of K-feldspar a coherent interface could develop along the plane of least coherency strain, $(\bar{6}01)$, so coherency by itself does not prove an origin by diffusion-controlled exsolution. However, the replacive albite was microporous, whereas film and braid perthites are strikingly pristine. The albite advanced into the K-feldspar along a front that was jagged, but this did not lead to a final product that was periodic. There can be no doubt that film and braid perthites form from an initially homogeneous parent by solid-state diffusion, and that the elastic properties of the continuous or largely continuous framework govern the orientation of lamellar interfaces (as shown by Willaime and Brown 1974) and the development and periodicity of twins (Willaime and Gandais 1972). They are therefore reliable markers of volumes of crystals that have not recrystallized since the microtexture formed. In an igneous rock such volumes are generally likely to have retained the bulk major, trace element and isotopic composition of the crystal at the time of its growth from magma. Perhaps the most striking illustration of the ability of these elastically strained structures to act as geochemical time capsules is that the microtexturally complex braid perthites at Klokken have retained almost all their radiogenic ^{40}Ar since emplacement at 1166 Ma, whereas deuterically coarsened regions with subgrain microtextures have lost as much as half of their ^{40}Ar over the same period (Parsons et al. 1988).

Intergrowths formed by replacement

The second broad type of perthitic intergrowth is formed by replacement. Pre-existing structure is dissolved and reprecipitated in an aqueous fluid by an interface-coupled process (Putnis 2002), which leaves the outline of the original crystal es-

sentially unchanged. The resulting crystal is a partial or complete pseudomorph. Replacive intergrowths are relatively irregular and in general considerably coarser than intergrowths produced by diffusion, up to several millimeter in macroperthites, which usually come from pegmatites. The most accessible indicator of replacement in feldspars (and other minerals) is the development of turbidity (Parsons 1978; Putnis 2002). Using LM in PPL at low magnification most alkali feldspar crystals from plutonic rocks have clear regions, which at higher magnification in appropriately orientated sections can often be seen to be composed of regular coherent intergrowths usually on scales <5 μm, and turbid regions in which intergrowths are considerably coarser, sometimes reaching millimeter-scales, and irregular in shape. The connection between turbidity and microtextural change was recognized by Andersen (1928) and re-emphasized by Parsons (1978). However, its profound character was not fully appreciated until the TEM work of Worden et al. (1990) on Klokken. We now know that single alkali feldspar crystals on 10 mm scales have often been partly or entirely replaced by a mosaic of Ab-rich and Or-rich subgrains, individually on scales ranging from a few tens of nanometers (Worden et al. 1990, Fig. 7b) to >250 μm, without any change in the morphology of the crystals in the igneous rock (Parsons and Lee 2009, Figs. 2, 6, and 9).

Replacement perthites can form in two broad ways. Isochemical dissolution-reprecipitation leads to no change in the bulk composition of the crystal and is driven largely by minimization of coherency strain energy, leading to fully, or largely, incoherent intergrowths (Worden et al. 1990; Brown and Parsons 1993). This process was termed mutual replacement by Smith and Brown (1988) and is often called "deuteric coarsening." Mechanisms of mutual replacement are treated by Parsons and Lee (2009) and Parsons et al. (2009). Replacement may also be demonstrably non-isochemical (e.g., Lee et al. 1995; Lee and Parsons 1997b; Plümper and Putnis 2009) involving exchange of the three feldspar components between crystals and fluids, driven by conventional differences in their chemical potentials, and leading to a change in the bulk composition of the crystal. Non-isochemical replacement often seems to occur after a phase of strain-controlled exsolution. Replacement is facilitated, but not primarily driven, by minimization of coherency strain and often begins at misfit dislocations which it must therefore post-date (Fig. 1b [3]; Lee et al. 1995; Lee and Parsons 1997a). Criteria for distinguishing mutual and non-isochemical replacement are given in the techniques section below. Norberg et al. (2013) have recently succeeded in converting a synthetic coherent cryptoperthite into a patch perthite, complete with micropores and subgrains, in the laboratory.

Replacive intergrowths are in general much coarser than coherent intergrowths, often on >100 μm scales. They usually have an irregular patch or vein morphology (Figs. 1 and 2). In contrast with strain-controlled intergrowths the interfaces between Ab- and Or-rich volumes are usually extremely irregular [e.g., in Klokken, Worden et al. (1990), Figs. 1 and 2; Shap, Lee and Parsons (1997b), Fig. 1; the type perthite from a pegmatite, Perth, Ontario, Parsons and Lee (2005), Fig. 10]. In most plutonic alkali feldspars, coherent and deuterically coarsened intergrowths occur together within the outlines of single crystals (e.g., Parsons 1978; Worden et al. 1990). The patches and veins themselves are composed of clusters of Ab-rich and Or-rich subgrains, with submicrometer-scale micropores at their junctions (Worden et al. 1990; Walker et al. 1995). Micropores often have the form of "negative crystals," sometimes with the adularia habit. Micropores are the main cause of the turbidity of feldspars and throughout the mineral world are commonly associated with dissolution and reprecipitation reactions (Putnis 2002). Pores do occur occasionally in pristine feldspar, and Burgess et al. (1992) showed that in Klokken they contained fluids with $^{40}Ar^*/Cl$ suggestive of a mantle origin, trapped during crystal growth, whereas fluids in turbid regions had lower $^{40}Ar^*/Cl$, probably because of evolution during boiling at lower *T*. Micropores in feldspars are a non-trivial feature of the Earth's crust; Johnson and Rossman (2004) calculated that in the upper crust they contain about the same amount of water as all the conventional hydrous minerals put together.

Individual subgrains often have the {110} + (010) habit characteristic of the low-*T* K-feldspar adularia and its Na equivalent pericline (Figs. 1b and 2a). These habits are a strong marker of replacement in feldspars, in a wide range of environments. Diamond-shaped {110} subgrains are common in Klokken (Worden et al. 1990; Walker et al. 1995; Parsons et al. 2013) where CL shows remarkable oscillatory chemical zoning within the subgrains (Lee et al. 2007b; Parsons and Lee 2009, Fig. 9). In Shap, subgrains with the adularia habit nucleate on misfit dislocations (Walker et al. 1995; Lee and Parsons 1997b; Fitz Gerald et al. 2006). They continued to form during diagenesis in detrital fragments incorporated in a Carboniferous conglomerate after the Shap pluton was unroofed (Lee and Parsons 1998). Subgrains with {110} habit are often associated with the replacive development of microcline from orthoclase (Waldron et al. 1993). We disagree with Sánchez-Muñoz et al. (2012, p. 1018) that "albite diamonds" in orthoclase can be produced by the "dry" coarsening of film lamellae. Their TEM micrographs (Fig. 14) show features that can be matched in many of our micrographs of Shap feldspars which are clearly replacive. In our view the evidence for extensive replacement in alkali feldspars is overwhelming. Some degree of microporosity is the norm in alkali feldspars and it marks a widespread crustal process with geochemical implications that deserve the attention of petrologists (Andersen 1928; Alling 1932; Parsons 1978; Putnis 2002; Putnis et al. 2007)

Patch perthites show their patch character most clearly when viewed on (001) (Fig. 2a) (also Parsons and Lee 2009, Figs. 4– 6). Patches are sometimes defined by {110} (Figs. 1b and 2a) and are "single-crystal" subgrains, but many patches can be shown, using TEM, to be mosaics of subgrains of the same phase, on a large range of scales (e.g., Worden et al. 1990, Fig. 7b). Viewed from directions close to **b** patch perthites form stubby, discontinuous columns or veins near the Murchison plane (Fig. 2c). Figures 2a and 2c illustrate very clearly the need to take account of orientation when describing perthitic crystals.

Vein perthites may be extremely irregular (e.g., Lee and Parsons 1997b, Fig. 1) or sub-periodic, with a strong preferred orientation (e.g., Parsons and Lee 2005, Fig. 10; Balić-Žunić et al. 2013, Fig. 2b; Yuguchi et al. 2011b). Surfaces are often stepped (e.g., Lee and Parsons 1997b, Fig. 2), and sometimes extremely intricate (Parsons and Lee 2005, Fig. 10). Common orientations are close to (100) and {110}. The former is close to the Murchison plane (see preceding section) suggesting that

replacement has followed the orientation of pre-existing semi-coherent film lamellae and that fluid has entered the crystal along misfit dislocations. Lee and Parsons (1997b, Figs. 2–4) show how replacement can develop along pre-existing semi-coherent film lamellae, with incoherent albite subgrains growing around what we now realize are nanotunnels (Fig. 1b). Alternatively, Norberg et al. (2011) found, in their experimental study of albitization of sanidine, that during the initial stage of replacement, coherent and semicoherent interfaces advanced into the sanidine parallel to ($\bar{6}01$), to minimize coherency strains. As replacement advanced a sub-grain mosaic developed. For replacement on {110} Smith and Brown (1988) favor a suggestion of Andersen (1928) that the fluid was exploiting contraction cracks.

"Ultraporous late feldspar," UPLF, corresponding with regions of extreme turbidity cross-cutting all earlier microtextures is a recent discovery in Klokken (Parsons et al. 2013, Figs. 11–15; present Fig. 2a). It is composed of Ab- and Or-rich patch intergrowths of near end-member composition (mean Ab_{97} and Or_{98}), implying very low-growth T (<170 °C). Subgrains are characterized by high concentrations of defects, and have distinctive complex, mottled diffraction contrast in TEM. A special feature of Klokken UPLF, not shared by replacement textures formed at higher T, is that it appears to form in a piecemeal fashion, so that "ghost" relics of prexisting microtextures can be seen in the diffraction contrast. Mottled strain contrast occurs in replacive albite in sedimentary rocks (Lee et al. 2003b) and in K-feldspar overgrowths on detrital feldspars (Worden and Rushton 1992; Lee and Parsons 2003; Parsons et al. 2005), suggesting it is a low-T phenomenon. However, it has been observed in feldspars subject to albitization at 450–350 °C (Engvik et al. 2008) and in experimental studies of replacement at 500 °C (Norberg et al. 2011) and 600 °C (Hövelmann et al. 2010) so it is not, of itself, proof of very low T. It should also be noted that very pure replacive albite (Ab_{99}) occurs in Shap (Lee and Parsons 1997b), again associated with extreme turbidity, but it forms very well-developed {110} subgrains with sharp boundaries against the enclosing orthoclase. There seem to be different styles of low-T replacement at work.

Applications of intergrowths formed by replacement

Both Klokken and Shap have experienced two stages of replacement and it seems likely that similar records of fluid-feldspar reaction events are common. Nakano et al. (2005, Fig. 2) provide a BSE SEM image of the development of patch microperthite from coherent film perthite in a feldspar from a Patagonian quartz syenite, which looks very similar to deuterically coarsened feldspar in Klokken, except that the average size of the patches, ~10 μm, is considerably less than Klokken, where individual Ab- or Or-rich patches are often 100 μm across [compare, e.g., Figs. 4 and 5 in Parsons and Lee (2009)]. The feldspars are of essentially the same composition. Perhaps the composition of the fluid is the controlling factor, or P at the time of the coarsening event.

Yuguchi and Nishiyama (2007) and Yuguchi et al. (2011a, 2011b) have suggested that the periodicity of vein (called by them "patch") intergrowths can be used to estimate relative cooling rates, but such intergrowths have a well-defined subgrain microtexture and clearly formed by replacement. Volume diffusion can be ruled out on kinetic grounds and it seems most unlikely that such intergrowths can be used to estimate cooling rates. This question is explored in the Discussion of Recent Alkali Feldspar Studies section below.

If ternary phase compositions in patch and vein intergrowths can be estimated using EPMA or quantitative EDS, two-feldspar geothermometry can be used to estimate the T of replacement, provided an estimate of P can be made (see section on thermochronology, below). The presence of strain-controlled film lamellae throughout large volumes of the Or-rich patches in Klokken (Fig. 2b [3]) is very good evidence that the patches have not changed in bulk composition since they formed. The presence of peristerite in Ab-rich patches provides similar evidence but, so far, we have found only one example (Parsons and Fitz Gerald 2011; Parsons et al. 2013). Abart et al. (2009b) and Tajčmanová et al. (2012) also reported examples of film lamellae post-dating a phase of coarsening in granulite facies rocks. In both Klokken and these studies the film lamellae represent a return to diffusion-controlled exsolution following a phase of fluid-mediated dissolution-reprecipitation. It seems likely that episodic diffusional and replacive exsolution are common.

In the case of Klokken, Brown et al. (1983) concluded that the patch perthites formed isochemically ("mutual" replacement) with respect to major elements. Their conclusion was reached after laborious traversing analyses using EPMA, of several crystals in a rock section. If the bulk analyses of several crystals are the same or closely similar it is reasonable to infer that replacement was isochemical, because the proportion of braid to patch perthite within individual crystals is very variable within a single section. However, as Brown et al. admit, it is very difficult to obtain reliable bulk analyses of coarse patch perthites by microbeam methods (see methods section below).

Parsons et al. (2009) used LA-ICPMS to measure a large range of trace elements as well as major elements simultaneously, with a beam size of ~20 μm, in a small sub-set of Klokken samples. While major elements were conserved, many trace elements, including REE, were lost to the fluid, and Pb and Sr were added in some crystals. Trace elements partition between the Or- and Ab-rich phases in the patch perthites so that $\log_{10}D^{Or/Ab}$ gives a straight line when plotted against ionic radius. The slope of this line is controlled by Na-K partitioning, which defines the average size of the T site in the two phases, and which in turn depends on solvus relationships. The trace element partitioning lines are therefore a geothermometer. Although not independent of conventional Ab-Or thermometers trace elements might provide useful evidence that feldspar pairs are in equilibrium in situations where there is doubt.

Mason (1982) studied partitioning of trace elements in coarse lamellar perthites from pegmatites using SIMS, also with a 20 μm beam. The albite lamellae were up to 100 μm wide, and Mason found that elemental distributions across the lamellae were curved, rather than flat as would be expected at equilibrium. He suggested that the lamellae were formed by diffusion but our experience is that such coarse lamellae are composed of subgrains, suggesting replacement. Volume diffusion can be ruled out on kinetic grounds. It would be interesting to investigate lamellae like those studied by Mason using the higher resolution of modern SIMS instruments, and to look at the detail of the microtexture with SEM and TEM.

Evidence of non-isochemical replacement

Significant variation in alkali feldspar crystal bulk compositions within a sample would be evidence of non-isochemical replacement, but is subject to the analytical problems discussed in the preceding section. A more reliable approach is to consider the chemical relationships of the different regions of microtexture. For example, in Shap (Lee and Parsons 1997b), a sub-solvus, two-feldspar granite, the bulk composition of the film cryptoand micro-perthite (Fig. 1a) is ~$Ab_{30}Or_{69}An_1$. This provides the best estimate of the bulk composition of the sanidine (now orthoclase) that crystallized from the magma at the same time as separate crystals of plagioclase, a calcic oligoclase, ~$Ab_{72}Or_2An_{26}$. *T* implications are discussed under Thermochronology, below. The vein perthite that cuts the film perthite (Fig. 1a) is composed of subgrains of microcline (~$Ab_{9.4}Or_{90.4}An_{0.2}$) and calcic albite (~$Ab_{89.8}Or_{1.5}An_{8.7}$) (Fig. 1b [2]). The film perthite adjacent to veins often appears depleted in albite film lamellae (Lee and Parsons 1997b, Fig. 1; present Fig. 1a) suggesting that some of the Ab in the veins came from the film perthite, but there is not enough An to account for the calcic albite in the veins. We concluded that the vein albite was largely introduced from outside the feldspar crystals. Subsequently, "pure replacive albite" ($Ab_{99.2}Or_{0.5}An_{0.3}$) (Fig. 1b [3]) precipitated around prexisting film lamellae, often nucleating on misfit dislocations. It is restricted to within about 1 mm of crystal margins, evidence that replacement was not isochemical, and the volume of Or-rich feldspar replaced may be high (Lee and Parsons 1997b, Figs. 2c and 3), ruling out a local origin for the albite within the crystals. Late albite of comparable composition replacing K-feldspar has been reported in several other studies (Ferry 1985; AlDahan et al. 1987; Ramseyer et al. 1992) and occurs in UPLF in Klokken (Parsons et al. 2013). AlDahan et al. (1987) suggested that Na released by sericitization (low-*T* growth of muscovite) in the separate plagioclase phase, led to the development of replacive albite, in the Siljan granite, and this is a possibility in Shap. Plümper and Putnis (2009) have also stressed the importance of sericite in replacive albitization.

Some degree of turbidity is the norm in feldspars from granitoids and this provides overwhelming evidence that replacement in alkali feldspars is commonplace. The reddening, sometimes intense, of feldspars in many granites is evidence of a major crustal process, as stressed by Putnis et al. (2007). However, attempts to correlate turbidity with bulk geochemical changes are few. In a comprehensive study of hydrothermal alteration in granites from the Isle of Skye, in which the feldspars are often exceptionally turbid, Ferry (1985) showed that a feldspar "turbidity index" (volume of turbid feldspar/total volume of feldspar) was correlated with decrease in $\delta^{18}O_{SMOW}$ from +8‰ in clear alkali feldspar to –6‰ in the most turbid. Ferry also noted that the clear feldspar analyzed by EPMA had a narrow range of compositions whereas the turbid feldspar was a mixture of analyses in the range $Ab_{99}Or_1$-Ab_5Or_{95}. Although there are no micrographs he suggested that the turbidity was caused either by "a myriad of tiny fluid inclusions" or by "a network of grain boundaries between coexisting albite and orthoclase produced during exsolution," a prescient description of patch perthite formation. In the case of one of the granites studied, Beinn and Dubhaich, MacKenzie and Smith (1962) had shown, using SXRD, that the clear feldspar was a cryptoperthite.

In Klokken, $\delta^{18}O$ has an essentially constant "mantle" value of 4–7‰ throughout the layered series irrespective of turbidity (Finch et al. 1995). Nevertheless in igneous layers in which alkali feldspars are turbid, coarse patch perthites (Worden et al. 1990) show along-strike variation in the major element bulk composition both of feldspars and mafic phases (Parsons and Becker 1986). This was ascribed to a deuteric fluid circulating at high *T* before the feldspars began coherent exsolution at >700 °C, and well before patch perthite formation at <500 °C. The potential for turbidity to be a marker of large-scale major, trace element and isotopic changes in rocks is clear.

The chemistry of felsic rocks provides some constraints on the scale of replacement. In a classic memoir, Tuttle and Bowen (1958) demonstrated the correspondence between normative *ab*, *or*, and *Q* in 571 analyzed granites with ≥80% normative *ab* + *or* + *Q*, and experimentally determined liquidus minima in the "haplogranite" system Ab-Or-Q. This work signaled the end of the "granitization" hypothesis, which postulated that granites were produced entirely by replacement (metasomatism) of preexisting rocks, and replaced it with a largely magmatist view in which much of the variability of granites could be accounted for by variations in the source and fractional melting, and/or by episodes of fractional crystallization during ascent and emplacement. The general disposition of phase volumes, cotectic surfaces and liquid lines of descent in the quaternary system Ab-Or-An-Q were deduced from acid volcanic rocks by Carmichael (1963) and provide a secure framework for the evolution of granite magma. Presnall and Bateman (1973) showed that its generation by fractional melting could be described in a similar way. The definitive work on fractionation in the ternary feldspar system with water is Brown (1993).

Since the early classics there have been many other experimental and field based studies that support the view that crystal-silicate liquid relationships dominate granite formation. Nevertheless, most data sets for individual composite intrusions show substantial scatter in both major and minor elements. It is possible that some of this scatter is caused by post-emplacement replacement. Nevertheless, the observation that most granites at least approximate to liquidus minima suggests that non-isochemical replacement is generally of limited extent and perhaps represents redistribution of feldspar components at a local scale.

Where non-isochemical replacement is postulated, the composition of the rock and its feldspar phases before and after the replacement event must be considered. Plümper and Putnis (2009), for example, made a careful and detailed study of sequential replacement reactions and porosity formation in feldspars in granitoids from SE Sweden. Their samples, which are from a large batholith, have clearly had a much more complex history of replacement than the small intrusion at Shap. While we agree with most of their interpretation there is one feature that seems to us incompatible with normal crystallization in granites. The dominant phase is microporous oligoclase (average $Or_1Ab_{72}An_{27}$) containing irregular islands of clear, non-porous microcline ($Or_{97–90}$ $Ab_{3–10}An_0$) which have the same optical orientation. They suggest that the microcline crystallized from magma (presumably as sanidine, because granite magmas normally crystallize well above the stability field of microcline) and was the dominant alkali feldspar until at some lower *T* it was pervasively replaced

by oligoclase by reaction with a late magmatic aqueous fluid. There was then a second phase of replacement, by relatively pure albite, accompanied by sericite, and, in some types, a final stage of replacement of sericite by a second K-feldspar, described as orthoclase.

Several questions arise. First, what sort of rock was present before the postulated large-scale replacement by oligoclase? For a very Or-rich sanidine to be an early crystallizing phase requires a K-rich magma composition, in the primary phase volume of sanidine in the system Ab-Or-An-Q. Silicate liquids of this composition are extremely uncommon as are rocks predominantly composed of orthoclase or microcline. Second, is the bulk composition of the rock "normal" for a granitoid? Is it near the "granite minimum" or on a plausible liquid line of descent from diorite? If so, how was this composition reached by a process of replacement? Plümper and Putnis (2009) do not provide rock analyses but some from the batholith are provided by Wahlgren et al. (2004). (This is a technical report of the Swedish radioactive waste agency, SKB, and can be accessed online.) The data are unfortunately not presented in a way that permits calculation of a CIPW norm but although there is considerable scatter (compatible with restricted replacement events), there are no features that suggest that the rocks do not form a normal igneous association. While the presence of microcline within the large plagioclase crystals perhaps suggests the order of events postulated, its association with regions of intense alteration (Plümper and Putnis 2009, Fig. 3) suggests to us that it is more likely that the microcline formed by late replacement of plagioclase.

Si-Al order-disorder, phase transitions, and twinning

Repeated fine-scale twinning (sometimes called "polysynthetic" twinning), on the Albite and Pericline laws, can occur only in triclinic feldspars. It is almost always developed, over a range of dimensions. Feldspar twin laws are discussed in detail by Smith and Brown (1988, Ch. 18). Repeated twins can develop during growth, in response to deformation, and as a result of phase transformations. Albite twins in plagioclase in basic igneous rocks and in plagioclase as a separate phase in two-feldspar granitic rocks will normally be growth twins. In alkali feldspars repeated twinning develops as a consequence of the ($C2/m$)–($C\bar{1}$) phase transitions: (1) the Si-Al ordering transition between sanidine or orthoclase and microcline, leading to the distinctive "tartan" or "cross-hatched" combined albite and pericline twinning and (2) the shearing transformation in Ab-rich compositions, between sanidine and anorthoclase. In coherent mesoperthitic intergrowths like Klokken, exsolution, ordering, and twinning are intimately coupled (see section on coarsening rates in braid microperthites). Framework ordering affects solvus curves, which in ordered frameworks are at ~100 °C higher T than when disordered. Parsons et al. (2010, Fig. 1) summarize the experimental data.

Order-disorder

Si-Al ordering and disordering are considerably slower than Na-K interdiffusion, shown very strikingly in heating experiments on alkali feldspar intergrowths in which TEM shows that features related to the Si-Al-O framework, such as twinning and tweed, persist near or even above the solidus for many hours after complete compositional homogenization (Parsons et al. 2010). MacKenzie (1957) showed that a continuous series of albites with different degrees of order could be made over a range of T, and that the feldspars intially grew with Si-Al disorder and then ordered with time. It is not clear whether natural feldspars behave in this way. Ordering rates in albite are relatively rapid and low albite was synthesized by Martin (1969) after only 14 days at 350 °C, in the presence of excess Na as $Na_2Si_2O_5$. There is evidence from similar experiments that ordering proceeds via a dissolution-reprecipitation reaction, and that the rate is sensitive to fluid composition (Mason 1979, 1980a, 1980b). The high albite-low albite phase transition was reversed at high P (1.8 GPa) by Goldsmith and Jenkins (1985) and can be deduced to be of similar form at lower P from other experiments (Brown and Parsons 1989, Fig. 1). The transition is continuous although intermediate albite is stable over a relatively narrow range of T, ~720–650 °C at 0.1 GPa in pure albite. The intermediate albite field intersects the equilibrium-order solvus at ~100 °C lower T.

Phase relationships and ordering rates are less securely known in Or-rich feldspars. The best estimate of the T of the sanidine-microcline transition, 480 ± 20 °C, is based on the conversion of microcline to orthoclase in the contact aureole of the Ballachulish granite in western Scotland (Kroll et al. 1991). It involves a heat-flow model of the intrusion provided by Buntebarth (1991). Microcline has not been synthesized in conventional experiments near this upper stability limit but assertions made in text-books that it takes extraordinarily long times to form, or indicates relatively low-crystallization T, are incorrect. In Klokken, fully ordered low microcline developed in 10^4–10^5 years (Brown and Parsons 1984a) on the basis of calculated cooling curves, and low microcline is growing in real time at 360–250 °C in the Salton Sea geothermal field, which has been active for only ~16 000 yr (McDowell 1986). The only reported synthesis of microcline is by Flehmig (1977) who found millimeter-scale crystals of microcline in hydroxide gels held at 20 °C and atmospheric P for 90 days in alkaline Na-Ca-K chloride solutions, essentially diagenetic conditions. As Brown and Parsons (1989) point out, there is no obvious reason why ordering in sanidine should be very much slower than in albite. Experimental work by Bertelmann et al. (1985) and Kroll and Knitter (1991) on ordering rates in sanidine supports this view.

The development of orthoclase in very large, slowly cooled intrusions and its persistence in some cases over billions of years, reflects the character of the monoclinic-triclinic phase transition, during which the tweed domain microstructure develops. Particularly well-developed tweed is shown in Fitz Gerald and Harrison (1993, Fig. 5) and by Sánchez-Muñoz et al. (2012, Fig. 13a). Tweed is not restricted to K-feldspar and occurs, for example, in peristerite in the Ab-rich phase of a Klokken patch perthite (Parsons et al. 2013, Fig. 10d). More strongly developed peristeritic tweed is illustrated by Janney and Wenk (1999). See Putnis and Salje (1994) for a general review of tweed microstructure.

The orthoclase-microcline transformation is reviewed at length by Smith (1974, Ch. 9), Smith and Brown (1988, Ch. 9), and Brown and Parsons (1989). As we stated above, orthoclase has ~80% of its Al in T_1 sites, whereas fully ordered low microcline has all its Al in the T_10 site. The character of tweed in K-feldspar was established by Eggleton and Buseck (1980) using

HRTEM. They calculated that strain energy in the tweed domain walls developed during ordering would eventually balance the decrease in free energy provided by further ordering within the domains. Thus the total driving force for ordering, once tweed has developed, is very small, and large, triclinic ordered domains (corresponding with Albite and Pericline twins in microcline) do not spontaneously develop. McLaren and Fitz Gerald (1987) showed, using convergent beam electron diffraction (CBED) and atom location by channeling enhanced microanalysis (ALCHEMI), that regions of tweed only 50 nm in diameter had triclinic symmetry, although the crystal was monoclinic using conventional SAED. It is the low driving force for coarsening of tweed that has led to the belief that ordering rates in K-feldspar are intrinsically low.

Further ordering requires an "unzipping" process (Brown and Parsons 1989) that removes the constraint of the tweed microstructure while maintaining and increasing order in the product feldspar. How this happens is not understood. In some cases it is clear that unzipping involves dissolution-reprecipitation in a fluid [e.g., the retrogressive microcline veins in granulite-facies orthoclase illustrated by Waldron et al. (1993, Fig. 3)]. Bambauer et al. (1989) introduced the term "irregular microcline" for a form with patchy, curving twins often demonstrably associated with replacement. In Shap, irregular microcline is found in relatively microporous veins associated with non-isochemical replacement of orthoclase (Lee et al. 1995; present Fig. 1b). Many plutonic K-feldspars are mixtures of orthoclase and microcline on a sub-μm scale (e.g., Fitz Gerald and McLaren 1982, Fig. 11), which may well be explicable in this way. Bambauer et al. (1989) found that in metamorphic rocks in the Swiss Alps and in the contact aureole of the Ballachulish granite, tweed orthoclase, irregular- and regular-microcline all occurred together within single crystals. Al in $T_1 0$ (obtained from cell parameters) increased progressively from orthoclase to regular microcline, suggesting that irregular microcline is an intermediate stage. In composite igneous plutons there is a strong tendency for microcline to be the dominant K-feldspar in the most evolved units, an observation consistent with a role for water in the phase transition (Parsons and Boyd 1971). However, although replacement is a common way for the orthoclase-microcline transition to occur it is not clear how a degree of order is communicated from reactant to product. "Unzipping" can also occur in response to deformation and Harker (1954, 1962) showed that microcline developed at the expense of orthoclase in progressively more deformed acid orthogneisses.

In the absence of direct experimental evidence the thermodynamic character of the M→T transition remains controversial. Brown and Parsons (1989, Figs. 6 and 8) considered it to be continuous, like that in albite, on the basis of a compilation of largely unreversed experiments and the observation that intermediate microcline occurs, albeit rarely, in nature. They proposed that intermediate microcline has a narrow region of stability in the range 500–420 °C analogous to that of intermediate albite (see above). They suggested that its rarity is a function of the rapidity of ordering when unconstrained by the development of tweed. Carpenter and Salje (1994) carried out an analysis of experiments on the ordering rate of sanidine by Kroll and Knitter (1991, see applications, below) using the Landau theory of phase transitions, and concluded that the transition was discontinuous (first order). However, the reversed experiments of Kroll and Knitter at 750 and 850 °C were well above the M→T transition, and the equilibrium degree of order in their experiments at 650 °C was inferred from ordering rates in these high-*T* experiments, leading to uncertainty in extrapolation into the region of the symmetry change at 480 °C. It is possible to synthesize both iron microcline ($KFeSi_3O_8$) and gallium microcline ($KGaSi_3O_8$) (Taroev et al. 2008 and papers therein) and the phase transition from Fe- and Ga-sanidine forms appears to be first-order. However there is also evidence that the ordered Fe-feldspars form from a disordered precursor by dissolution-reprecipitation, accompanied by porosity formation (Walker 1991) so the order of the phase transition remains ambiguous.

Twinning

Triclinic microcline is almost always twinned in a "cross-hatched" or "tartan" pattern. The observation that the Albite and Pericline twin composition planes are at 90° led Laves (1950) to suggest that microcline formed from a monoclinic precursor. In SXRD patterns obtained from appropriately orientated fragments using film methods (Smith and MacKenzie 1955; MacKenzie and Smith 1962; Smith and Brown 1988, Fig. 6.4) the combined twins give rise to distinctive clusters of four spots, often streaked, sometimes with a fifth diffraction from monoclinic orthoclase at their center. Similar clusters can be imaged using SAED in a TEM (Fitz Gerald and McLaren 1982, Fig. 2). In principle, such features could be mapped in reciprocal space using modern area detectors as promoted by Balić-Žunić et al. (2013), but they did not report them (see later). There is great variation in the appearance of the twinning on both LM and TEM scales. The most comprehensive review is Fitz Gerald and McLaren (1982). They showed from SAED patterns that in many cases what appear morphologically to be Pericline twins are in fact composed of structure related by the Albite law. However, for practical purposes it is adequate to retain the term Pericline twin, because when formed they were composed of structure related by this law. Sánchez-Muñoz et al. (2012) provide some striking LM images of relatively regular twinned intergrowths.

The mechanism of formation of the regularly twinned varieties of microcline is unclear. Some (e.g., Fitz Gerald and McLaren 1982, Fig. 12) are regularly organized orthoclase-microcline intergrowths, suggesting a continuous, diffusion-controlled process involving coarsening of a tweed precursor. An unusual style of "tiled" twinning was found in microcline in a nepheline syenite from the Ilimaussaq intrusion by Smith and McLaren (1983), which may have formed during direct growth as a triclinic phase from a very low-*T* magma. The existence of ordered, untwinned adularia in low-*T* environments, the real-time growth of Albite and Pericline twinned microcline in the Salton Sea system (McDowell 1986), and the synthesis experiments of Flehmig (1977) all suggest that microcline can form directly and relatively rapidly under the appropriate conditions. There is an urgent need for a systematic study of the microtextures of microcline in a range of well-defined geological contexts.

In some circumstances the tweed problem is sidestepped by interaction with a perthitic Ab-rich phase. In Klokken braid microperthites exsolution began in an Ab-rich sanidine and the intergrowth was initially of two monoclinic phases (Brown and

Parsons 1984a). Albite twinning in the Ab-rich phase formed when its composition reached the intersection of the coherent solvus and the M→T shearing transformation (Fig. 2b [1] and [2]). The *T* of this intersection depends on ternary composition and on framework ordering and hence on cooling rate. The twins initially had long periodicity (λ_{twin}), which decreased during cooling, and low obliquity. Twin obliquity and λ_{twin} and are coupled by coherency strain with the thickness of the exsolution lamella (Willaime and Gandais 1972). As the Or-rich phase orders, the dominant triclinic Ab-rich phase dictates its "left"-"right" sense of order and interfaces adopt a zigzag configuration (Fig. 2b [1]), eventually maturing into the "diamond" microtexture of braid by rotation toward $\{\bar{6}\,\bar{6}1\}$ (Fig. 2b [1] and [2]). The zigs and zags are deformed twins in an orientation called the diagonal association, because their SXRD spots are in a position intermediate between those produced by albite and pericline twinning (Brown et al. 1972). There is at present no experimental or theoretical way to calibrate the rates of these coupled processes.

In straight film lamellae, if lamellae continue to coarsen after twinning λ_{twin} adjusts to local lamellar thickness (Fig. 1b [1]) as predicted by Willaime and Gandais (1972). Brown and Parsons (1984a) concluded that primary coarsening did not occur after twinning in Klokken braid intergrowths because λ_{twin} is independent of local lamellar widths (the diamond-shaped $\{\bar{6}\,\bar{6}1\}$ columns in the braid texture in Fig. 2b [2]). In Shap, λ_{twin} increases with lamellar thickness, as does the spacing of misfit dislocations (Lee et al. 1995, Fig. 5). Pericline twins in albite film lamellae in Shap are close to the high-albite position, which can be explained if the effect of ~1% An is taken into account (Fitz Gerald et al. 2006). As Smith and Brown (1988, p.530) explain, once a Pericline twin has formed its composition plane will remain in the same orientation although decreasing *T* and increasing order mean that the rhombic section changes orientation. In plagioclase it is possible to recognize intersecting twins of different generations. Deuteric perthitic intergrowths seem usually to form at ≤500 °C (Lee and Parsons 1997a; Parsons et al. 2013) so twins in Ab-rich subgrains must form by growth in the low-albite field. In film lamellae in Or-rich patches in Klokken, Albite twin periodicity is a function of lamellar thickness (Fig. 2b [3]; Parsons et al. 2013, Fig. 9) showing that twin widths have adjusted as coarsening proceeds. Sánchez-Muñoz et al. (2012) and Parsons et al. (2013) provide examples in which the development of twins in microcline is related to coherent interfaces with Albite twins in perthitic albite lamellae.

Applications of order-disorder and related twinning

In volcanic rocks attempts have been made to relate Si-Al order in sanidine to cooling rate calculated from geological considerations. Scott et al. (1971) studied low sanidines in the range $Ab_{23–27}Or_{72–75}An_{1–2}$ from a thick (300 m) ignimbrite from Nevada which had $2V_x$ between 0 and 42°. Ordering and visibility of exsolution textures varied with height in the ignimbrite, those in the center being the most ordered and most visibly exsolved. They used heat loss models to calculate approximate cooling times down to 500 °C, and obtained values of 100–200 yr near the base and top and up to 450–650 yr in the center. Equivalent equilibrium temperatures calculated from ordering experiments on Eifel sanidine by Bertelmann et al. (1985) vary from ~550 °C in the center to ~730 °C at the top and bottom. Thus, sanidine crystals in the ignimbrite must have ordered considerably more slowly than those from the Eifel.

Sanidine crystals from the Eifel region have some remarkable and important properties and have been much studied, because they have a considerable bearing on the potential of Si-Al ordering as a "geospeedometer." A summary (including many references) is in Parsons and Lee (2005). The most studied material comes from a tuff at Volkesfeld, erupted from the Laacher See volcano 12 880 yr ago. It has a bulk composition of $Ab_{15}Or_{85}$ but is glass-clear, devoid of exsolution textures and tweed, and has been shown by several methods to be extraordinarily perfect, with dislocation densities of $<10^6$ cm^{-2}. It is a high sanidine, with optical axial plane parallel to (010) and $2V$ between 0 and 20°. Its most remarkable property is that its degree of order (non-convergent ordering, the fraction of Al in T_1 sites, see above), measured by $2V$, varies rapidly and reversibly when heated "dry" at different *T*, reaching an equilibrium value in a few hours at 1050 °C and in 100–200 h at 750 °C (Bertelmann et al. 1985). It was also found that the rate of change in $2V$ decreased with prior heating. This loss of reactivity was studied by Bernotat-Wulf et al. (1988), who showed that ordering and disordering rates were fastest in the center of thick slabs (>2 mm) and decreased toward their margin. The loss of reactivity started at the edge of the slab and moved inward with time, and was accompanied by the development of irregular pores, some containing fluid, in the (010) plane. It is reasonable to deduce that the pores form by exsolution of water from the feldspar structure, and that this component exercises a strong control on Al-Si interdiffusion. Subsequently, Graham and Elphick (1990) showed, in experiments on ordering rates in albite, that the active species was structural H^+ (protons).

Kroll and Knitter (1991) investigated the ordering kinetics of two sanidines from Volkesfeld and like Bertelmann et al. (1985) found that preheating slowed ordering rates. Degree of order was estimated from $2V$ and they obtained reversals at 850 and 750 °C in 10 and 100 days, respectively. At 650 °C the untreated natural sample ordered further, and an equilibrium degree of order was inferred from the higher *T* experiments. Equilibrium would be reached after several years. They proposed a model for calculating rock cooling paths and considered that the ordering kinetics of their preheated sanidine were more "normal" (their term) than those of the unusually reactive crystals studied by Zeipert and Wondratschek (1981) and Bertelmann et al. (1985). However it might be argued that, in Nature, in the *T* range in which sanidine is stable, the very perfect Eifel material is more "normal."

If an ephemeral species like H^+ has a profound effect on ordering rates it may be difficult to use Si-Al order as a geothermometer or as a measure of cooling-rate unless some independent way can be found of estimating a_{H^+} during ordering. Although Na↔K interdiffusion seems not to be sensitive to water content or pressure (evidence reviewed by Yund 1984), in some styles of exsolution, such as braid formation, it is intimately coupled to framework ordering (see above). It is therefore possible that the linear relationship between stratigraphic height and log λ in Klokken is to some degree a function of the water content of the magma at the time of crystal growth (Brown et al. 1983). There are two inter-bedded types of syenite in Klokken, which shared exactly the same thermal history during exsolution and

coarsening. One type formed as a roof-chill sequence at the roof of the fractionating syenitic magma chamber, the other formed as a cumulate in the more evolved, water-rich magma that was the end product of fractionation. The two types lie on different height/λ lines, with the later feldspars having approximately twice the lamellar periodicity of the early series at any height. Brown et al. suggested that this could reflect incorporation of an H^+ species. However, an uncompleted FTIR study of extremely perfect, glass-clear regions in both syenite types (Parsons and Fitz Gerald, unpublished) did not show any systematic correlation between "water" concentration and syenite type, although the wave-number spectra of the two types are distinctive. Extreme care was taken to avoid possible fluid inclusions or films of hydrous phases in fractures, but it is perhaps unlikely that feldspars would retain their structural "water" unmodified for 1166 Ma.

The Ab-rich feldspar phase in perthitic alkali feldspars in most plutonic igneous and metamorphic rocks is low albite or, in crystals with higher An, low oligoclase, and sometimes andesine. Ordering is so rapid in albitic plagioclase that it does not provide an indicator of cooling rate. The discovery of a peristerite intergrowth in the Ab-rich phase of a patch perthite from Klokken (Parsons and Fitz Gerald 2011; Parsons et al. 2013) opens up the possibility of using such intergrowths as a guide to cooling rate. Peristerites form only in ordered frameworks (Carpenter 1981). Cooling curves for Klokken (Brown and Parsons 1984a) suggest that coarsening of the peristerite was completed within 10^5 yr of crystallization. It seems most unlikely that this example is unique, and there is evidence from clastic albitic feldspars in sedimentary rocks that peristerite may be more common than usually believed (Lee et al. 2003b). It would be worthwhile to look at albitic feldspars in range of granites, both as a separate plagioclase phase or as Ab-rich subgrains in deuterically coarsened perthite, using TEM.

Early attempts were made to relate degree of order in plutonic Or-rich feldspars to cooling rate or rock type, using the separation of paired PXRD reflections such as 131 and $1\bar{3}1$ (Δ_{131}), which depends on the obliquity, and hence degree of convergent order in triclinic feldspars. A single 131 reflection occurs in monoclinic feldspars. Dietrich (1962) gave a histogram of Δ_{131} values for no less than 500 alkali feldspars from a wide range of geological settings which established the bimodal character of K-feldspar, with the overwhelming majority having Δ_{131} <0.2 (orthoclase) or >0.8 (near to low microcline). He used the width of the broadened 131 reflection to estimate Δ_{131} in orthoclase which is unlikely to be related to short-range convergent ordering in tweed. Extensive SXRD data summarized by MacKenzie and Smith (1962) also showed the bimodal character of orthoclase and microcline. Cell parameters refined from PXRD patterns were used by Stewart and Wright (1974) (222 samples from a wide variety of sources) and Guidotti et al. (1973) (139 samples from regional metamorphic rocks) to estimate the fraction of Al in T_1 sites. Feldspars with monoclinic diffraction patterns (orthoclase) had ($t_1$0 + t_1m) (the fraction of Al in the T_1 sites) covering a considerable range but concentrated around 0.8, whereas triclinic feldspars (microcline) overwhelmingly have ($t_1$0 + t_1m) >0.9, mostly >0.95. Stewart and Wright found that about one third of their samples had cell parameters indicating structural strain, with cell volumes corresponding with compositions determined by EPMA but with the **a** cell dimension larger than in unstrained samples. They correctly ascribed the strain to coherency with exsolved albite. Kroll and Ribbe (1987) provided equations for estimating site occupancies from cell parameters with high precision, based on diffraction patterns obtained from 38 K-rich feldspars for which the Al contents of the tetrahedral sites had been estimated from T-O bond lengths obtained by crystal structure refinement. They also provided quantitative strain indexes to take account of coherency strain in perthitic intergrowths.

Contrary to the assertion of Balić-Žunić et al. (2013) that their XRD methods can be used for "analysis of crystal intergrowths on another still largely missing level where no routine approaches have developed so far," there exists a considerable body of high-quality PXRD and SXRD work, some of it based on full crystal structure refinement, which provides a secure foundation for the TEM and SEM work that has become the preferred technique for microtextural characterization. Balić-Žunić et al. mention strain only once, in an erroneous statement on p. 50, and coherency is never mentioned.

As discussed in the previous section it is generally accepted that the bimodal character of ordering in K-feldspar is a result of "unzipping" of tweed microtexture in partially ordered orthoclase leading directly to highly ordered microcline (Brown and Parsons 1989). Unzipping occurs most commonly during fluid-feldspar reactions. Microcline formation can also be directed by external strain and by coherency strain imposed by albitic lamellae. In braid mesoperthites coherent coupling with a dominant volume of triclinic albite causes intermediate microcline and ultimately low microcline to form continuously from sanidine. Although a considerable effort was made by early workers to use estimates of degree of order for petrological purposes, the modern view is that it is related more to these unzipping processes than to factors such as cooling rate or crystallization *T*. It is uncertain whether measuring the average degree of order in Or-rich plutonic feldspars has any useful petrogenetic significance.

TEM shows that many crystals that appear using OM to be microcline are orthoclase-microcline mixtures (Fitz Gerald and McLaren 1982). For igneous rocks early PXRD work (Parsons 1965) showed that the relative proportions of orthoclase and microcline varied systematically between different units of a composite syenitic intrusion, with microcline predominating in the most evolved members, and Parsons and Boyd (1971) and Parsons (1978) extended this finding to a range of intrusions. This observation most probably reflects buildup of magmatic water during igneous evolution, with the same fluid facilitating unzipping of orthoclase in the microcline field.

Thermochronology of microtextures

The time-temperature (*t*-*T*) evolution of microtextures, which may include multiple stages of dissolution-reprecipitation in an aqueous fluid, can be assessed semi-quantitatively by using a combination of the cross-cutting relationships of the different microtextures and *T* estimates using ternary solvus relationships. Temperatures of the beginning of exsolution by diffusion, and of replacement events, estimated by Parsons et al. (2013) for Klokken, and Lee Parsons (1997b) for Shap, and are given in Figures 1 and 2. Analytical methods for obtaining the necessary compositional data are given in the next section.

For feldspars with negligible An, binary solvus curves can be used to estimate minimum crystal growth *T*, using the strain-free solvus, and the beginning of coherent exsolution on the coherent solvus. Parsons et al. (2010, Fig. 1) compiled the following curves: Smith and Parsons (1974), strain-free solvus for disordered feldspars; Bachinski and Müller (1971), strain-free solvus for ordered feldspars; Brown and Parsons (1984a), interpolated strain-free solvus for feldspars with equilibrium order based on data from Müller (1971); Sipling and Yund (1976) coherent solvus for disordered feldspars; Yund (1974) coherent solvus for ordered feldspars.

For ternary feldspars, estimates of the equilibration *T* of feldspar pairs or temperatures at which the ternary solvus is intersected may be made reliably only for feldspars with Si,Al disorder. Two-feldspar geothermometers can be accessed using the computer package SOLVCALC (Wen and Nekvasil 1994). It is straightforward to insert new values of mixing parameters into this package. Crystallization *T* of feldspar pairs on tie-lines on the ternary solvus can be calculated. If a single feldspar phase is present solvus isotherms can be calculated at an appropriate *P* and its minimum growth *T* inferred. The most used thermometers are Fuhrman and Lindsley (1988) and Elkins and Grove (1990). Benisek et al. (2010a) have recently provided a thermometer based on calorimetry which is probably the best choice for feldspar pairs with more than a few percentages of An. Its isotherms are in excellent agreement with high-temperature feldspar pairs from Kokken (Parsons and Brown 1983). However, on the Ab-Or join it leads to a solvus at *T* below the experimental synthesis solvus of Smith and Parsons (1974), thought to be caused by short-range Na-K ordering (clustering) in the vicinity of the binary solvus (Benisek et al. 2014). The other thermometers give similar results for low concentrations of An, closer to the experimental solvus, but, as Benisek et al. (2010a) show, are not in good agreement with natural assemblages in which both members have relatively high An. It is important to take account of even low concentrations of An. Because of the steep shape of the ternary solvus, low concentrations of An have a large effect on the *T* at which exsolution begins. Sections of the ternary solvus for Or-rich feldspars, calculated using Elkins and Grove (1990) are given by Parsons et al. (2009, Fig. 9). 1 mol% An raises the solvus *T* of feldspars covering the range of most granites ($Ab_{30}Or_{70}$–Or_{100}) by ~300 °C. A more recent calorimetric study of the Or-An join by Benisek et al. (2010b), suggests that this may be an underestimate.

There are no experimental determinations of ternary coherent solvi, for either ordered or disordered frameworks. The best estimates can be made by adjusting *T* obtained from the thermometers above by amounts inferred from the coherent and/or ordered binary solvi (Parsons et al. 2010, Fig. 1). The inferred equilibrium-order strain-free solvus (Brown and Parsons 1984a) is ~80 °C above the experimental disordered strain-free solvus (Smith and Parsons 1974). The experimental disordered coherent solvus (Sipling and Yund 1976) is ~60 °C below, in good agreement with the calculated coherent solvus of Robin (1974). Pressure raises the critical *T* of the binary strain-free solvus by 22 °C/100 MPa (Hovis et al. 1991), but its effect on coherent solvi is not known. An estimate of the *T* of the beginning of exsolution of the peristerite found in a Klokken mesoperthite was made by Parsons and Fitz Gerald (2011) based on the "conditional spinodal" of Carpenter (1981). The effect of *P* is again not well known.

In summary, the steepness of the ternary solvus, lack of exact data on both its strain-free and coherent shape, the role of Si-Al ordering and the effects of *P* conspire to introduce considerable uncertainties in interpreting phase compositions (e.g., Lee and Parsons 1997b; Parsons et al. 2009), even when coarse enough for EPMA analysis. Nevertheless, although it is difficult at present to infer exact *T*, relative *T* can be shown to correspond with the order of events in the formation of the most complex microtextures (e.g., Parsons et al. 2013).

In Klokken (Fig. 2) the highest *T* recorded by alkali feldspar pairs is 970 °C based on TEM work on coexisting meso- and crypto-perthites in adjacent crystals in an alkali gabbro (Parsons and Brown 1983; Benisek et al. 2010a). The main phase of coherent exsolution in the syenites, leading ultimately to braid perthite began at ≥700 °C, depending on An content. The first phase of mutual replacement, giving patch perthite (Figs. 2a and 2b), occurred after microcline formation in braid perthite, at ~500 °C, and was followed by nucleation of film perthite in Or-rich patches which occurred between 460 and 340 °C, depending again on their bulk composition (Parsons and Lee 2009; Parsons and Fitz Gerald 2011; Parsons et al. 2013). The presence of strain-controlled film lamellae throughout large volumes of the Or-rich patches is very good evidence the patches have not changed in bulk composition since they formed. At some lower *T*, misfit dislocations formed on film lamellae and finally UPLF developed at <170 °C, over-printing all earlier microtextures (Parsons et al. 2013).

It is important to consider the effect of both An content and structural state on the *T* at which exsolution begins. In an An-free feldspar $Ab_{30}Or_{70}$, coherent exsolution would begin at ~600 °C in a fully ordered framework (Yund 1974) and at ~440 °C if fully disordered (Sipling and Yund 1976) (see also Parsons et al. 2010, Fig. 1). In Shap, Pericline twins in film albite lamellae are close to the high-albite position (Fitz Gerald et al. 2006), rotated slightly toward low albite (Fig. 1c), suggesting that the disordered coherent solvus defined the beginning of exsolution. In the An-free system this would have been in the low-albite field. However, the bulk An content of the Shap film perthite is 0.8 mol% and the extreme sensitivity of the ternary solvus to low concentrations of An implies that coherent exsolution would have begun at ~600 °C, in the intermediate albite field (Fitz Gerald et al. 2006, Fig. 5).

In the coarse, incoherent vein perthite in Shap (Fig. 1), which cuts across the coherent intergrowths (Fig. 1a) the mean composition of the phases imply *T* of 385 °C, using the two-feldspar geothermometer for disordered feldspars of Fuhrman and Lindsley (1988). The ordered solvus would imply ~490 °C (Lee and Parsons 1997a). Microcline formed from orthoclase during replacement and this *T* is within the range of the M→T transition recommended by Kroll et al. (1991).

In principle, replacive events could occur long after original crystallization, as proposed in the context of $^{40}Ar/^{39}Ar$ thermochronology by Parsons et al. (1999).The deuteric patch perthites in Klokken and the vein perthites in Shap could, in principle, have formed at any time in the subsequent history of the feldspars. In

the case of Klokken there is strong geological evidence (summarized in Parsons et al. 1988) and mineralogical evidence (Parsons and Fitz Gerald 2011) that all the microtextures illustrated in Figure 2 formed during initial cooling of the intrusion, at 1166 Ma, within ~10^5 yr after crystal growth. A possible exception is UPLF in which the coexisting Ab- and Or-rich phases have compositions very close to the end-members, implying growth below ~130 °C. In a recent study of UPLF from Klokken, Harrison et al. (2010), employing a ^{40}K-^{40}Ca dating method using SIMS, have claimed that replacement continued episodically until ≤719 Ma and perhaps as late as ~400 Ma. In the case of Shap there is evidence from ^{40}Ar/^{39}Ar work that all events recorded in the microtextures, including late replacement by very pure albite, occurred soon after emplacement (Short et al. 2011).

Recommended routine methods

To characterize alkali feldspar microtextures adequately it is usually necessary to apply a range of imaging techniques. With the exception of TEM, the techniques discussed below do not require specialist skills and use routine equipment available in many laboratories. While TEM is often the most informative method it is usually necessary to select an area of interest in a conventional thin section using LM or at an intermediate scale in a polished section in an SEM, using BSE. Chemical analysis can be combined with BSE imaging in most modern EPMA instruments and SEMs. To get the best out of any of these techniques we strongly recommend use of orientated sections or fragments.

Sample orientation

Because of the low symmetry of alkali feldspars and the microtextural complexity of examples from plutonic rocks we strongly recommend viewing samples using LM, SEM, and TEM from known orientations. In a thin section of an igneous rock without a preferred fabric it is better to concentrate on a few crystals in orientations that can be deduced from the features we give here than to look at large numbers of randomly orientated grains. Perthitic intergrowths can look very different viewed from different directions, giving a false impression of great variability. With respect to feldspar microtextures approximate viewing directions and scales should be given for all micrographs, for all imaging techniques.

The most informative viewing directions for all microscopic techniques are normal to the two "perfect" cleavages in feldspars, (001) and (010), which are at right angles at a macroscopic scale in almost all alkali feldspars. Cleavage fragments can be produced by light crushing (we use a miniature piston-cylinder device), selected using a binocular microscope and glued to a glass slide on their most conspicuous cleavage. This is usually either (001) (Figs. 1a–1b and 2a–2b) or (010) (Figs. 1c and 2c).

For fragments lying on (001) a second perfect cleavage defining the fragment will most probably be (010), although less perfect {110}, (100), and ($\bar{2}$01) partings are also reported. A common plane of fracture, the "Murchison plane" (see earlier), close to ($\bar{6}$01), is near (100) and perhaps accounts for partings reported in that orientation. Because ($\bar{6}$01) is at right angles to (010), fragments lying on (001) often have a rectangular outline. Film lamellae may be visible in non-turbid parts of fragments and will be at right angles to the (010) cleavage and parallel to the Murchison fracture.

Fragments lying on (010) (Figs. 1c and 2c) are usually defined by the (001) cleavage and the Murchison plane. They have a rhombic outline because ($\bar{6}$01) makes ~110° with the (001) cleavage. Film lamellae are parallel to ($\bar{6}$01). Note that these two figures are at very different scales. The fragment in Figure 1c might be <4 μm measured along **a**, whereas that in Figure 2c is perhaps 400 μm in the same direction.

Light microscopy (LM)

We strongly recommend Chapter 19 in Smith and Brown (1988) for an overview of perthitic intergrowths viewed using LM. Exsolution lamellae and twins can be imaged in thin sections at scales down to ~500 nm if care is taken with orientation and illumination. Cleavages and Albite twins are the quickest guide to orientation in most plutonic feldspars, although cleavages may be only weakly developed in volcanic feldspars and twins are at sub-LM scales in cryptoperthites. Standard ways of obtaining optical orientation are given in textbooks. The most effective way of estimating the average degree of Si-Al order in monoclinic alkali feldspars is to measure the optic axial angle, $2V_\alpha$, using LM (Su et al. 1986). Orthoclase has $2V > 50°$.

Albite twinning, in both albite and microcline, is parallel to the (010) cleavage and if the cleavage and the twin composition plane are sharply defined the viewer is looking from a direction near the **a**–**c** plane. Polysynthetic twinning parallel to any good cleavage is almost certainly Albite twinning, because Pericline twinning, which is visible from the **b** direction, is parallel to the (001) cleavage only for special compositions and/or structural states (Fig. 1c). If the Or-rich phase is microcline, combined Albite and Pericline twinning will be sharply defined (using XP) in sections near (001) because Pericline twins are almost normal to (001) (Fig. 1c). In Ab-rich volcanic feldspars (anorthoclase) combined Albite-Pericline twinning is visible in sections near (100) because the Pericline twin composition plane is near the high-albite position (Fig. 1c). The Pericline twins shown in the albite lamella in Figure 1c are at sub-LM in scale and are unlikely to be confused with anorthoclase.

In most plutonic igneous rocks the two broad types of perthitic intergrowth can be easily differentiated in thin section, strain-controlled in clear areas and deuteric in turbid areas (Parsons 1978). The patch or vein character of deuteric intergrowths can be seen either in PPL (e.g., Figs. 3a and 3b in Parsons et al. 2013), when the Ab- and Or-rich phases may be differentiated by the higher relief of the former, or using XP when twinning becomes visible. Thick sections can display the outlines of subgrains using XP (Parsons and Lee 2009, Fig. 3). Turbidity around film lamellae can often be seen in PPL and is often a precursor to more pervasive replacement (Fig. 1b [3]) (Lee and Parsons 1997b).

Common assertions in the literature that clear areas in plutonic alkali feldspars are "unexsolved" using LM are certainly incorrect unless the bulk composition of the crystal is extremely close to the Or-rich end-member. Visibility is a function of both the coarseness of the exsolution texture and its orientation and fine microperthitic and cryptoperthitic intergrowths are not uncommon in plutonic K-feldspars. Random sections of fine-scale exsolution textures are uninformative and they are best viewed either approximately normal to (001) or to (010). Albite

film lamellae in cross-hatched microcline may be hard to see using XP on (001) (e.g., Fig. 3c in Parsons et al. 2013) because they are almost parallel to Pericline twins (Fig. 1c). The relief difference in PPL makes them visible. Repeated twinning is usually sub-LM in the Ab-rich phase in film perthites. Coarser braid textures are visible, with care, using PPL and XP in sections near (001) when they have the appearance of intersecting threads in a diamond pattern. They often coarsen near crystal margins and along prominent cleavages to give "pleated rims" [illustrated by Brøgger (1890)], which are related to the initiation of the deuteric coarsening process (Lee et al. 1997). The Ab-rich phase in perthites almost always exhibits Albite and Pericline twinning (Figs. 1b and 2b), but the twinning is usually sub-LM in coherent intergrowths.

Scanning electron microscopy (SEM)

For routine characterization by SEM (or EPMA) we recommend embedding mm-sized cleavage fragments, defined by conspicuous parallel cleavage surfaces, in resin so that they rest on one of the cleavages. This is likely to provide a family of fragments lying predominantly on (001) and (010) surfaces, which can usually be recognized using the criteria in sample orientation above, and are the most informative viewing directions. SE images of freshly cleaved surfaces can show subtle features such as Albite and Pericline twins but are not an effective way of revealing exsolution textures. The morphology of micropores can be examined at high magnification. They often have negative-crystal shapes and contain grains of non-feldspar phases that may be qualitatively analyzed using EDS (Walker et al. 1995) or identified from crystal shapes using TEM (Worden et al. 1990; Putnis et al. 2007).

Using a BSE detector the atomic number contrast (Z-contrast) of the Ab- and Or-rich phases can be seen on freshly prepared cleavages, but images are usually better from polished surfaces, which are also suitable for fluorescent X-ray analysis in the SEM or for EPMA. Most micrographs show Ab-rich feldspar dark and Or-rich feldspar bright, although it is worth pointing out that this can be reversed at the microscope. Variations in gray-scale (used qualitatively in Figs. 1 and 2) are sensitive guides to compositional variation. In Klokken for example, the contrast between Ab-rich patches ($\sim Ab_{91}Or_1An_8$) and Ab-rich UPLF ($\sim Ab_{97}Or_2An_1$) can be clearly seen (Fig. 11 in Parsons et al. 2013). The best viewing surface for coherent intergrowths is (001) because zigzag and braid textures are visible which appear straight or slightly wavy on (010). Film lamellae appear straight on both planes and lamellae <100 nm thick can be imaged. Random sections of braid textures often give wavy or lenticular patterns, depending on the angle between the intergrowth and the plane of section. Waldron and Parsons (1992) discovered lenticular bulk compositional fluctuations, which they called "ripples," in braid cryptoperthites from the Coldwell syenite (also a larvikite) which caused changes in the BSE signal on scales of ~100 μm, although λ of the underlying cryptoperthite, only faintly visible in the BSE image, was on the order of 100 nm (measured using TEM).

The contrast between strain-controlled and deuteric microtextures in crystals in which intergrowths have been partially coarsened is very striking in BSE images (e.g., Worden et al. 1990; Parsons and Lee 2009). At low-magnification micropores are visible as black dots. These are usually at subgrain boundaries and triple junctions (Walker et al. 1995) that are not visible if the subgrains are composed of the same phase. The correlation of micropores with deuterically coarsened areas, and their almost complete absence from regions with coherent intergrowths, is clear (e.g., Parsons et al. 2005, Fig. 10). Deuteric intergrowths have an irregular "patch" or "vein" morphology viewed on (001), and form ragged "veins" near (010) (Fig. 2c; Worden et al. 1990; Parsons and Lee 2009, Fig. 4b). Other orientations occur. Veins near (110) are common in feldspars from pegmatites. Individual Ab- and Or-rich subgrains can sometimes be distinguished on (001) because they have the {110} habit of adularia (Figs. 1b and 2a; Parsons and Lee 2009, Fig. 6). The best developed patch perthites occur in syenites (such as Klokken) and nepheline syenites (our unpublished observations). Well-developed vein perthites are characteristic of hypersolvus granites in which the feldspars have slightly more Or-rich bulk compositions than in syenites (Lee et al. 1997, Fig. 7). In all these rock types it is common for entire crystals to have been replaced; they are true pseudomorphs. Usually it is possible to find relics of a braid precursor (Parsons 1978, Fig. 7 and many later papers on Klokken) although these may be uncommon (Lee et al. 1997, Fig. 7). Film albite lamellae in Or-rich patches that formed subsequent to deuteric coarsening (Figs. 2a and 2b [3]) can be imaged using BSE (Parsons et al. 2013, Fig. 2).

In alkali feldspars from subsolvus granites, low-*T* deuteric coarsening often begins at misfit dislocations (Fig. 1b [3]; Lee and Parsons 1997, Figs. 2–4). The existence of dislocations is best confirmed using the etching technique (below, 4) or TEM (6). At low magnifications (in both BSE and LM images) the first stages of deuteric coarsening appear as a roughening of the surfaces of film lamellae (Lee and Parsons 1997, Figs. 1–3). If, at higher magnification, the roughness can be seen to be periodic it is likely that dislocations are involved. Small lamellae and platelets between more obvious lamellae (Fig. 1b [1]) may also be visible. Replacive veins in Shap (Figs. 1a and 1b) are not related to dislocations because replacement occurred at ~410 °C before dislocations formed. Pure replacive albite (Fig. 1b) formed at low *T* after dislocation formation.

Secondary electron (SE) imaging of etched and weathered surfaces

Etching of cleavage surfaces in HF vapor can reveal fine detail without the need for sectioning and polishing. Waldron et al. (1994) give practical details. The etching process is something of a black art, related perhaps to humidity and the local speed of air flow in your fume cupboard, and can be difficult to control. Over-etching results in loss of detail, and we recommend starting with short etching times of ~10 s. Albite lamellae usually etch more slowly than K-feldspar, and the resulting relief provides resolution of a few tens of nanometers, high enough to show details of fine-scale film and braid textures. Regions with coherency strain etch more rapidly so that shallow trenches develop along lamellar interfaces. A particular strength of the method is that it reveals misfit dislocations on the interfaces of semicoherent exsolution lamellae (Waldron et al. 1994, Figs. 3 and 4). Etch-pits form quickly during etching and have twofold symmetry viewed on (010) and mirror

symmetry on (001) as demanded by the *C*2/*m* space group. They are distributed periodically along the length of exsolution lamellae and are rare or absent on small lamellae. They occur in pairs normal to the long axis and each pair is a section of a single dislocation loop encircling a very flat, lenticular exsolution lamella. Most etch pits form on pre-existing nanotunnels (Fitz Gerald et al. 2006) and etching can enlarge pull-apart cleavages connecting the opposite sides of the dislocation loop, giving etch pits with an hourglass shape. Repeated twins can be revealed (Parsons and Lee 2005, Fig. 11) together with subgrain boundaries (Parsons et al. 2013, Fig. 4).

Natural weathering reveals microtextures in much the same way as laboratory etching, and illustrates the importance of feldspar microtextures in natural dissolution and mechanical degradation during soil formation (Lee and Parsons 1995; Lee et al. 1998), sedimentary transport and diagenesis (Lee and Parsons 1998; Parsons et al. 2005). Microtexture exercises control on the way feldspars fracture, which affects the reactive surface area of particles, influencing dissolution rates in the laboratory (Hodson et al. 1997). It has been suggested that honeycombs of naturally enlarged nanotunnels would have provided ideal protected environments for the origin of life (Parsons et al. 1998).

X-ray microanalysis by EPMA or SEM

LM is often used for locating sites for EPMA but the microscope optics are often of poor quality for detailed microtextural work. BSE imaging is now a common precursor to EPMA analysis and can be used to target particular elements of a microtexture with precision. Here we make some comments on analytical strategies appropriate for complex intergrowths. The most fundamental distinction is between measurements of bulk composition, which may be of entire crystals or particular regions of crystals, or measurement of phase compositions. When the composition of a "K-feldspar" is stated it is essential to say whether the analysis includes perthitic albite, and is therefore the bulk composition of the K-feldspar, or whether perthitic albite has been deliberately avoided to provide an analysis of the Or-rich phase. If the latter is the objective it is important to check, using SEM (many modern EPMA instruments can be used in SEM mode) or TEM, that there are no fine-scale albite lamellae below the resolution of the EP light optics.

From a petrological standpoint point analyses of individual phases in intergrowths are in general less interesting than the bulk compositions of whole crystals or of distinct microtextural regions of crystals. Phase compositions and their structural state can be deduced from cell parameters even in very fine-scale intergrowths using SXRD and PXRD. Methods are reviewed in detail by Smith and Brown (1988, Ch. 6 and 7). Coherency strain must be taken into account. In volcanic rocks and small high-level intrusives, in which intergrowths are too fine-scale for EPMA, XRD shows that phase compositions can depart significantly from the end-members, for kinetic reasons, but in plutonic alkali feldspars ternary solvus relationships demand that the Ab-rich phase is near the pure Ab end-member, or close to the Ab-An join. In all equilibrium feldspar pairs the Or-rich phase has lower An and more Ab than there is Or in the Ab-rich phase. Spot analyses of any plutonic alkali feldspar that are far from the Ab and Or corners of a ternary plot (e.g., Harrison et al. 2010, Fig. 1; Yuguchi and Nishiyama 2007, Figs. 11 and 12; Yuguchi et al. 2011, Fig. 6a; Słaby et al. 2012, Fig. 8b) are mixtures of phases. The large compositional range of the Na- and K-rich phases in the intergrowths in sample 14 of Balić-Žunić et al. (2013, Table 3 and Fig. 2a), which we infer to be coherent, is likely to be an artifact of a large beam size (5 μm) relative to the microtexture (only the coarsest lamellae approach 10 μm), and a surface that is oblique to the lamellae.

Using a small diameter beam, EPMA can be used to obtain phase compositions at scales greater than a few micrometers, although care must be taken to avoid volatilization of alkali ions. Coherent and semicoherent albite film lamellae are often <1 μm in thickness and cannot be analyzed by EPMA. It is important to recognize that the excitation volume of the electron beam is considerably larger than its nominal diameter, and to bear in mind the three-dimensional shape of the intergrowths below the plane of the section. Sections in which the interfaces between phases are parallel to the beam direction are desirable. Only in granulite facies rocks (Evangelakakis et al. 1993; Cayzer 2002; Abart et al. 2009b) are coherent intergrowths coarse enough for reliable EPMA analysis of both phases.

Care must also be taken when interpreting element distribution maps, especially when the orientation of the microtexture with respect to the surface is unknown. In general such maps add little to the understanding of microtextures and usually merely confirm what can be deduced from BSE imaging or from etched surfaces. Particular care must be taken when interpreting color gradations in elemental images as indications of chemical zonation. For example, Abart et al. (2009b, Fig. 4) suggest that their albite "spindles" (see earlier comment) are zoned with respect to Ca, and this may be the case, but it is essential to take account of the excitation volume of the electron beam, which will inevitably lead to apparent gradations at the margin. The beam diameter is not given. If the albite bodies are indeed spindles then the electron beam would show a compositional gradation because it will penetrate through the spindle near its edge.

The bulk chemical composition of entire microtexturally complex crystals is probably most reliably obtained by analysis of crystal separates using X-ray fluorescence (XRF) analysis, although this is now rarely done. Bulk analyses of relatively fine-scale lamellar intergrowths can be obtained using EPMA with a defocussed beam, provided the beam diameter is considerably larger than the exsolution microtexture. Bulk composition of coarse intergrowths can be obtained using traversing or rastering, but this may be very laborious (Brown et al. 1983). Brown et al. (1983) concluded that Klokken feldspars had undergone isochemical mutual replacement, but there is still considerable intercrystal variation within each thin section (Brown et al. 1983, Fig. 1). Marks et al. (2003) used automated image analysis to obtain the proportions of the phases in BSE images of coarsely exsolved mesoperthites, in combination with point analyses of phase compositions, to calculate bulk compositions. It is doubtful whether such methods can be applied to fine-scale intergrowths.

Transmission electron microscope (TEM) imaging

The first TEM study of a cryptoperthite, a moonstone from Ceylon, was by Fleet and Ribbe (1963). This early transmission work was done on the thin edges of tiny fragments and was hit-and-miss. Etched surfaces were studied using a carbon-replica technique (Rosenqvist 1965; Aberdam 1965). Electron-transpar-

ent foils are now produced by thinning conventional thin sections using Ar-ion bombardment or by cutting wafers normal to surfaces using a focused ion-beam (FIB) (Heaney et al. 2001; Lee et al. 2003a, 2007a; Wirth 2004). Lee (2010) provides a review of modern preparation methods and also outlines the very large range of TEM techniques now available. Very small areas (a few micrometers across) can be targeted using these methods but for work on feldspar microtextures it is essential to select regions of interest in a lower magnification context, either using LM, or, if a polished thin section is used, BSE imaging in an SEM. For routine work we strongly recommend starting with (001) or (010) sections (see sample orientation above), gluing grids (usually 3 mm diameter) to polished sections for conventional ion-thinning of carefully pre-selected areas. An element of luck is involved in whether the desired area of interest will been retained in the thinned area. The FIB method has the advantage that areas of interest can be targeted very exactly but the disadvantage that the wafer is cut normal to the sample surface so that the likely three-dimensional configuration must be taken into account. The FIB technique is particularly effective for the study of naturally weathered and experimentally reacted feldspar surfaces (Lee et al. 2007a, 2008) although great care must be taken to avoid damaging the surface with the Ga^+ ion beam.

As well as providing bright- and dark-field diffraction contrast images, TEM has the advantage that SAED patterns may be obtained from very small selected volumes. Like the SXRD patterns used in the pioneering work of Smith and MacKenzie (1955) [examples are reproduced in Smith and Brown (1988), Fig. 6.4], SAED shows clusters of diffraction spots corresponding with the intergrown Or- and Ab-rich phases, with pairs of spots representing twins in various orientations. Monoclinic and triclinic phases may be readily identified, together with streaking of spots, streaks between spots and short-period Albite twin superstructures. Examples of SAED patterns of perthitic crystals can be found in Parsons and Brown (1983) and Brown and Parsons (1988), of orthoclase and microcline in Fitz Gerald and McLaren (1982), and of peristerite within a perthite in Parsons et al. (2013). Cell dimensions and angles may be measured directly (with useable precision) on diffraction patterns from carefully orientated crystals. The orientation of twins and lamellar features can be determined, and streaking of diffraction spots caused by coherency and by tweed microtextures examined. Very small changes in crystal orientation can be readily detected and heterogeneity in any elastic strain recognized.

Analytical TEM (ATEM) can be used for analysis of very small volumes but great care must be taken to avoid damage by the electron beam and take account of variations in sample thickness. Janney and Wenk (1999) describe the difficulties in a careful study of peristerite intergrowths in plagioclase. ATEM can provide useful chemical analyses of alkali feldspars with a beam diameter of 150 nm (Parsons et al. 2013) and major element distributions can be mapped at extremely small scale (<100 nm) in TEMs fitted with electron-energy-selecting column optics (energy-filtered TEM, EFTEM) (Parsons et al. 2010).

Other methods

Methods described in this section have been used in several studies but do not, in our view, for different reasons, qualify for inclusion in our list of recommended routine techniques.

Cathodoluminescence (CL) imaging

Cathodoluminescence is light, mostly although not entirely in the visible spectrum, produced by the interaction of an electron beam with a crystal structure. Although the color is sensitive to major elements and can be used to distinguish feldspar microtextures it is not as effective as BSE imaging for this purpose. It is used primarily to map trace element distributions or defects associated with them (Finch and Klein 1999; Götze et al. 2000). CL imaging may be carried out in various instruments over a range of scales, using polished sections. An early application of CL to feldspar studies was provided by Parsons and Brown (1983) using a home-made vacuum chamber and electron gun attached to a conventional optical microscope. Emission spectra can be obtained from areas of a few tens of micrometers using optical-CL systems and higher-resolution images can be obtained in SEMs equipped with a photomultiplier detector. The latter images are, in general, panchromatic. The most sophisticated CL images are "hyperspectral" (Lee et al. 2007b) and obtained using an electron probe fitted with a CCD spectrograph that produces a two-dimensional map in which each pixel, with a point spacing of only 0.5 nm, is a complete CL spectrum for wavelengths from 350 to 850 nm (larger than the visible spectrum). With this instrument the contribution of particular wavelengths to the CL spectrum can be investigated, and related to multiple CL activators.

In general we recommend that CL is done in the context of previous BSE work which provides a map of major element variation. In most SEM and EPMA instruments it is straightforward to change between the two operating modes. Examples from Klokken are given by Lee et al. (2007), Parsons et al. (2008), and Parsons and Lee (2009; Fig. 9 is a striking color image). These micrographs show complex, oscillatory chemical zoning in subgrains in Klokken patch perthites and illustrate the potential of CL for revealing microtextures related to trace elements (in this case Ti) that cannot be easily imaged by other methods. However, without the context provided by the BSE images these CL images would have been extremely difficult to interpret. Another shortcoming of CL as a technique is that the nature of activators, which may be major or trace elements, or point defects, or point defects associated with the site of trace elements, is not always clear (Finch and Klein 1999; Götze et al. 2000)

Electron backscatter diffraction (EBSD) and orientation contrast imaging (OC)

In our view EBSD and OC imaging (Prior et al. 1999) are intrinsically ill-suited to the study of the fine-scale microtextures that are the subject of the present paper, although they have a useful role in studies directed at feldspar deformation fabrics and the development of relatively large subgrains (e.g., Prior and Wheeler 1999; McLaren and Reddy 2008; Menegon et al. 2008, 2013). The geometry of the EBSD method is described very clearly by Prior et al. (1999). The orientation of the sample is calculated by matching the EBS pattern of the target region with a simulated pattern based on the symmetry and independently determined lattice parameters (both determined in feldspars by XRD) for the target mineral. These simulated patterns are collectively called "match units." In principle EBSD should be able to identify most feldspar microtextures (exsolution textures and repeated twins) that can be seen using LM.

McLaren and Reddy (2008) list reasons why this is not achieved. EBS patterns for feldspars are complex because of their low symmetry and are similar between different feldspar phases. There are many twin laws associated with various types of pseudo-symmetry. McLaren and Reddy tested a range of potential match units and selected monoclinic orthoclase (although their LM images clearly show that some of their K-feldspar is Albite and Pericline twinned triclinic microcline) and monoclinic albite, a phase that can exist only above ~1000 °C and cannot be quenched to room *T*. These choices can be rationalized as representing the average structure of twinned triclinic Na- and K-feldspars, and McLaren and Reddy were able to achieve the restricted objective of automatically mapping the Ab- and Or-rich phases in their sections with ~10 μm resolution, and compare the maps with conventional BSE (Z-contrast) images with considerably higher resolution.

Presumably evidence of the microtextures with which we are concerned in the present review might be found in the fine structure of the EBS pattern, but as far as we know this possibility has not been explored. It could be interesting to adjust the match units in line with, for example, the effects of coherency demonstrated by Stewart and Wright (1974) and Ribbe (1979). In general terms, without such refinements, EBSD analyses seem unlikely to contribute much to the understanding of feldspar microtextures.

Discussion of recent alkali feldspar studies

Several recent studies provide examples of the need for very careful orientation, attention to previous work and microscopic investigation over a range of scales, using appropriate techniques, if misinterpretation is to be avoided. We here provide what we hope will be seen as constructive comments.

Balić-Žunić et al. (2013)

Our present review was prompted by the publication of a paper by Balić-Žunić et al. (2013) entitled "Full analysis of feldspar texture and crystal structure by combining X-ray and electron techniques" in which the authors present "an integrated procedure for the micro-texture analysis, twin law identification plus crystal structure refinement of all components in a feldspar intergrowth." The claimed purpose of their work "was to establish analysis of crystal intergrowths on another still largely missing level where no routine approaches have developed so far" and to "attempt to overcome the textural obstacles," but they largely ignored the great body of historical characterization and interpretation of microtextures and as a result came to erroneous conclusions. They state that TEM is used for "nanoscopic high-resolution" in the study of feldspar. To the contrary, although TEM can image the feldspar lattice (Eggleton and Buseck 1980; Brown and Parsons 1984a, 1984b; Sánchez-Muñoz et al. 2012), much of the most useful TEM information about feldspars is gathered nearer the 1 μm scale. It is our view that the relatively simple microscopic and microanalytical techniques recommended in the present paper are considerably more reliable and informative than those applied by Balić-Žunić et al. (2013).

Balić-Žunić et al. (2013) employed many techniques in their study: PXRD followed by Rietveld analysis, EPMA, SXRD using an automated four-circle diffractometer with area detectors, BSE and EBSD in an SEM with simultaneous elemental mapping using EDS. Data derived from the EBSD patterns are presented in several ways to display both chemical and orientational relationships. LM was also used for some rudimentary examination. We here examine the success of their approach.

Balić-Žunić et al. (2013) studied two feldspars (samples 16 and 45) from larvikitic syenite pegmatites from the type locality near Oslo. Sample 16 is described as gray in color and 45 as light red. Both have similar bulk compositions, ~$Ab_{60}Or_{40}$. They make only one reference to the substantial body of previous work on feldspars from syenites, citing only an early review by Parsons and Brown (1984). In fact feldspars from the Larvik syenite have a classic status in the development of feldspar mineralogy. Feldspars from this general locality, with strong blue "schiller" ("iridescence" in the terminology preferred by Smith and Brown 1988) were the subject of one of the earliest TEM studies of any cryptoperthite (Rosenqvist 1965). He studied carbon replicas of (001) and (010) cleavage planes etched using HF. Rosenqvist also studied feldspars from a red variety of the syenite called tönsbergite. He found that the iridescent feldspars contained "perthite strings" 10 μm long with thicknesses of 0.1 μm, in an orientation that accounted for the iridescence. He also found regions of fine perthite in the tönsbergite but noted that there were also homogeneous domains 100 to 1000 times larger than in the blue feldspars. Rosenqvist had discovered the cause of feldspar iridescence and recognized deuteric coarsening 35 yr before the details of this process were examined in feldspars from the Klokken larvikite by Worden et al. (1990) using TEM. Nearly 50 yr after Rosenqvist's work Balić-Žunić et al.'s (2013) modern instrumentation did not lead to recognition of these important features.

LM and BSE. Balić-Žunić et al. (2013) provided no orientation information for their micrographs, complicating comparison with other samples. They provide one light micrograph (their Fig. 7), of sample 45, between crossed polarizers. The diffuseness of the interfaces of the microtextures in the image indicates that the section is oblique to all features of interest and although the authors state that it shows two phases both twinned on the Albite law, it is very difficult for the reader to confirm this. A section cut parallel to (001) would have provided all the evidence required to sustain the arguments of their paper.

The BSE image of sample 16 (Fig. 2a in Balić-Žunić et al. 2013) shows regular exsolution lamellae with an apparent λ generally below 10 μm. The viewing direction is unclear because no cleavages are visible. The fine scale, slightly sinuous lenticular shape and smooth surfaces of the lamellae strongly suggest that they are coherent film intergrowths viewed on a surface close to (001) or (010). It is possible, however, that the microtexture is that of a "braid" perthite viewed from near the *b*-axis. Examples of the contrasting appearance of braid intergrowths viewed on (001) and (010) are provided by Parsons and Lee (2009, Fig. 4). The bulk sample is described as "gray-green" in color, and we can discern no micropores in Figure 2a suggesting that it is relatively pristine, transparent feldspar, unaffected by fluid-feldspar reactions.

Feldspar sample 45 has a much coarser microtexture of irregular lamellae with complex interfaces on 100 μm scales (Balić-Žunić et al. 2013, Fig. 2b). Two cleavages are visible, at the left and at the top of the fragment. The angle between them is ~110°, strongly suggesting that the viewing direction is close to **b**. The overall orientation of the thick exsolution lamellae is therefore close to (100), confirming the conclusion of Balić-Žunić et al. (2013) based on EBSD. The irregular, stepped interfaces of the lamellae suggest that the microtexture is composed of clusters of Or-rich and Ab-rich subgrains. Parsons and Lee (2009, Fig. 4) provide BSE images showing deuteric intergrowths in a larvikitic feldspar from two orientations, one of them along **b**. The "light red" color of sample 45 suggests that it is turbid, with sub-micrometer micropores (Worden et al. 1990) probably containing hematite (Putnis et al. 2007). Much higher magnification would be required to see micropores in Balić-Žunić et al. (2013) Figure 2b. We conclude that Balić-Žunić et al. (2013) Figure 2b shows a deuterically coarsened vein intergrowth. Our suggestion that the coarse lamellae are built of subgrains could be confirmed by using either TEM (see e.g., Worden et al. 1990), or the HF etching technique of Waldron et al. (1994)

SXRD and PXRD. Although Balić-Žunić et al. (2013) makes no reference to earlier XRD work, SXRD, using film methods and orientated cleavage fragments, formed the basis of the earliest systematic studies of perthites, summarized by MacKenzie and Smith (1962). Examples of photographs are given by Smith and Brown (1988, Fig. 6.4). Instead of arrays of single diffraction spots they show clusters corresponding with the intergrown Or- and Ab-rich phases, and the twins in each phase. Early PXRD work showed that phase compositions can be obtained, accurately enough for most purposes, from single PXRD peaks, but corrections must be made if the phases are coherent. PXRD can also simultaneously provide an estimate of the degree of Si-Al ordering, most effectively in the triclinic phases (Stewart and Wright 1974).

Peak overlap and broadening is commonplace in PXRD patterns of perthitic feldspars. Parsons (1978, Fig. 4) gave examples from coherent and incoherent larvikitic feldspars. Peaks not only overlap but individual peaks are intrinsically broad for many reasons: coherency between the exsolved phases; coherency between twins; tweed microstructures; chemical gradients; local variations in Si-Al order, sometimes within both Ab- and Or-rich phases; mixtures of monoclinic and triclinic structure in the Or-rich phase. Although Balić-Žunić et al. (2013) mentions ways to work with peak overlap, they discuss none of the complicating factors and coherency is never mentioned. Stewart and Wright (1974) showed that coherency strain affects the **a** cell dimension most, because it is the dimension that differs most between Na- and K-rich feldspars. Cell volumes remain consistent with the compositions of the intergrown phases but cell edges are significantly different to those of single-phase feldspars of the same composition.

The diffraction methods promoted by Balić-Žunić et al. (2013) provided

large data sets which they matched to the patterns of standard single crystals or to calculated diffraction patterns. Cell parameters were calculated from the strongest parts of the diffractions using the Rietveld method with apparent high precision, but in so doing Balić-Žunić et al. (2013) discarded a large quantity of information about crystal microtexture, contained in the lower intensity parts of the broad diffractions. Starting parameters for all three diffraction methods used by Balić-Žunić et al. (2013) were those of simple, single-phase standard feldspars. These might be applicable to coarse sample 45, but they would not be appropriate for sample 16.

Balić-Žunić et al. (2013) collected data for ~1000 diffractions from unorientated single-crystal fragments, and calculated cell parameters, but they detected only a few of the microtextures likely to occur in their samples. They showed that both samples required more than one reciprocal lattice. Sample 16 was composed of one untwinned Or-rich phase and an Albite twinned Ab-rich phase. In 45, four orientations, representing two phases with Albite twinning, were detected. Pericline twinning was not detected in the low-microcline phase, which in our experience is most unusual. We also remark that the textures detected by Balić-Žunić et al. (2013) were extraordinarily simple for larvikitic feldspars (compare Parsons et al. 2013).

SXRD intensities were used for a crystal structure refinement by Balić-Žunić et al. (2013) (their Fig. 8). This is perhaps the only part of their study that must be carried out using XRD rather than EM. Again, Balić-Žunić et al. (2013) do not refer to any earlier work, although the effect of coherency strains on such measurements was studied by Ribbe (1979), also using a sample from a larvikite. He used 893 reflections to refine mean T-O distances in strained intermediate microcline intergrown with lamellar albite on a sub-micrometer scale (shown in a TEM image), taking great care to eliminate 204 overlapping peaks. He concluded that estimates of ordering could be obtained reliably from the cell parameters of Stewart and Wright (1974), despite considerable distortions. Ribbe's T-O distances appear on Figure 3.6 in Smith and Brown (1988). The equivalent points for Balić-Žunić et al. (2013) sample 16 plot in almost exactly the same places.

Although film is not used for SXRD today, its potential remains. The contemporary equivalent to film, the solid-state area detector, could be used to collect similar information extremely efficiently, as software could be used to orientate the crystals to generate the most easily interpreted diffraction patterns. Balić-Žunić et al. (2013) did not do this. Instead, as with PXRD, they used the automated SXRD methods to select only the strong diffraction maxima of the full reciprocal sphere, thus discarding all information on the character and orientation of phase boundaries and the distribution of twins. Their study is thus considerably less sophisticated than that of Ribbe (1979).

EBSD. Support for our interpretation of the contrasting microtextures of samples 16 and 45 comes from the EBSD work of Balić-Žunić et al. (2013). They could find "single phase grains" only in 45. This is consistent with the presence of a fine-scale coherent microstructure in 16 and unstrained subgrains in 45. The 3° range of orientations in 45 (Balić-Žunić et al. 2013, Fig. 9) can be accounted for by a mosaic of slightly misaligned subgrains (Worden et al. 1990, Fig. 7). The Or-rich phase in 16 is described as "orthoclase" or "partially ordered intermediate microcline," whereas that in 45 is "ordered low microcline." The Or-rich phase in straight coherent mesoperthites is usually monoclinic orthoclase with a tweed microstructure, but is intermediate or low microcline in braid intergrowths (Brown and Parsons 1988). Or-rich subgrains in deuterically coarsened feldspars are most commonly low microcline [as in Balić-Žunić et al. (2013) 45], rarely orthoclase (Parsons et al. 2013).

Balić-Žunić et al. (2013) present map data derived from the EBSD patterns but because the surface studied was randomly orientated and oblique to all microtextures of interest, the maps are extremely difficult to interpret. EBSD is complicated for low-symmetry phases such as feldspar and it is unsurprising that Balić-Žunić et al. (2013) had difficulty in interpreting their data, particularly for sample 16. Their EBSD work suggests that the exsolution lamellae in 16 are parallel to (010) which they acknowledge was "unexpected." Coherency on (010) is highly unlikely given the work of Willaime and Brown (1974) on minimization of coherency strain energy. In an over-simplified form, because the cell edge that differs most between Na- and K-feldspars is **a**, the smallest strains exist in coherent interfaces approximately normal to **a**, like the $(\bar{6}01)$ plane common in lamellar microperthites. The plane (010) suggested by Balić-Žunić et al. (2013) is the least likely orientation for an interface. Simple LM could have been adequate to establish the relationship between the lamellae and the (010) cleavage (see Recommended Routine Methods [2]). We again conclude (see Methods [8]) that the EBSD method is unsuitable for the study of complex, coherent intergrowths.

General conclusions. We fail to see in the approaches used by Balić-Žunić et al. (2013) much potential either to simplify or improve on existing methods for studying complex alkali feldspars. Balić-Žunić et al. (2013) set out to "attempt to overcome the textural obstacles" but instead have overlooked much of the critical information about geological history illuminated by the microtextures. They have missed parts of the microtexture and have reached some wrong conclusions [viz. lamellae orientated in (010) in sample 16]. The results (e.g., for unit-cell parameters) are compromised by the limitations of their "integrated" approach. Finally, far from representing a simple alternative, the approach they proposed requires lengthy and iterative data analysis, specialized skills and costly equipment, to produce results of limited applicability.

The exsolution microtextures in Balić-Žunić et al.'s (2013) feldspars differ greatly in scale, with λ from <10 μm in 16 to ~100 μm in 45. Our detailed interpretation of their sample 16 (their Fig. 2a) is that it is an oblique view of a coherent film or braid intergrowth, formed by diffusion. We interpret sample 45 (Balić-Žunić et al. 2013, Fig. 2b) to be a deuterically coarsened patch or vein intergrowth formed by dissolution-reprecipitation in a fluid. The color difference of the two feldspars is a very strong clue to their underlying microtextures, as Rosenqvist (1965) noticed. To account for the large difference in scale of the intergrowths in 16 and 45 Balić-Žunić et al. (2013) refer to a TTT diagram in Parsons and Brown (1984, Fig. 13) showing cooling curves for Klokken, and inappropriately select two which they consider represent the different cooling histories of their samples. The TTT diagram used applies only to fine-scale, coherent intergrowths with maximum λ <300 nm, much smaller than the λ of feldspars 16 (maximum ~10^4 nm) and 45 (10^5 nm). Coarsening kinetics for development of film perthites have been discussed recently by Parsons and Fitz Gerald (2011). It would take tens of millions of years to produce a 100 μm intergrowth, like that in 45, by diffusion. The microtextures in Balić-Žunić et al. (2013) samples formed by different mechanisms, but have experienced identical thermal histories and give no information on comparative cooling rates.

Yuguchi and Nishiyama (2007) and Yuguchi et al. (2011a, 2011b)

These authors made a very large number of measurements of the separations of perthitic film albite lamellae in alkali feldspars with bulk compositions near $Ab_{20}Or_{80}$ from two Japanese granites. The parameter measured was actually the thickness of the K-feldspar between opposing surfaces of albite lamellae and is therefore very slightly less than λ as defined in the present paper. Measurements were made using LM, and it is likely that sub-optical lamellae were missed. Sections were randomly orientated which will inevitably lead to an overestimate of λ. Yuguchi and Nishiyama (2007) studied samples from different topographic heights in the Okueyama body and Yuguchi et al. (2011a, 2011b) studied variation of λ with depth in boreholes in the Toki granite, sunk in connection with the Mizunami Underground Research Laboratory for study of radioactive waste disposal. In both intrusions they found a simple linear relationship between λ, in the range 5–20 μm, of albite film lamellae, some shown to be semicoherent (Yuguchi and Nishiyama 2007, Figs. 5a-1), and position, ascribing this to heat-loss through the roof of the intrusions. In both, the fractional downward increase in λ is small, barely greater than the 2σ errors given, and the author's choice of distances to be measured [Figs. 5 and 7 in Yuguchi and Nishiyama (2007) and Fig. 4 in Yuguchi et al. (2011b)] seems to be subjective. For example, Figure 5(b-1) in Yuguchi and Nishiyama (2007), appears to be based on only the larger lamellae in the plane of the section. Roughening of the surfaces of film lamellae suggests possible deuteric coarsening, and small lamellae and platelets appear to be present between more obvious lamellae. We suggest that these microtextures deserve study at higher magnification before conclusions are reached. The authors do not comment on the difference between their linear height/λ relationships and the log-linear relationship, and proportionally much larger range of λ, found in Klokken by Brown et al. (1983), which was also ascribed to cooling at the roof.

Very surprisingly Yuguchi and Nishiyama (2007) and Yuguchi et al. (20011b), also showed a similar variation in λ of deuteric vein lamellae (called by the authors "patch perthite lamellae") and position in the same granites with λ ranging from <50–200 μm. Bearing in mind the three-dimensional shape of the very irregular "lamellae" it is hard to see how a meaningful periodicity can be measured. They again ascribe the increasing downward spacing to decrease in cooling rate, but offer no suggestions as to how this relationship can arise by a replacement process. The LM images suggest that deuteric coarsening is being guided by pre-existing film lamellae, as noted previously in Shap (Lee and Parsons 1997, Figs. 2–4) but we do not have an explanation for the preferential deuteric coarsening.

The authors' estimates of the *T* of the beginning of exsolution are based on a misunderstanding of the phase relationships controlling coherent exsolution. Yuguchi and Nishiyama (2007) estimated 710 °C and Yuguchi et al. (2011a) 780 °C for the beginning of exsolution but both estimates are based on two-feldspar geothermometry. They were obtained using the bulk composition of their "film"

alkali feldspar intergrowths and coexisting plagioclase and represent the growth *T* of feldspars from magma coexisting at the ternary feldspar solidus-strain-free solvus intersection. Coherent exsolution would have begun at a substantially lower *T* when or after the homogeneous alkali feldspar intersected the ternary coherent solvus. The *T* of the beginning of coherent exsolution depends on the bulk composition of the crystal and is strongly sensitive to An content (see e.g., Parsons et al. 2009). In an An-free feldspar of composition ~$Ab_{20}Or_{80}$, exsolution would be at ~450 °C, using the coherent solvus for ordered feldspars of Yund (1974). At this *T* the cooling times of 800 yr at the roof and 1390–1890 yr 1000 m below suggested by Yuguchi and Nishiyama (2007) on the basis of a one-dimensional heat transfer model are much too short to develop λ of ~5–10 μm (their Fig. 5b-2). The approximation $x^2 = Dt$ (see section above on coarsening rates of film microperthite) implies annealing at 450 °C for between ~10^5 and ~10^6 yr. "Film" lamellae in the Toki granite (Yuguchi et al. 2011a), with λ >15 μm, would require annealing for >10^6 yr, and applying this reasoning to the coarsest deuteric vein lamellae in Yuguchi et al. (2011b) (λ 50–200 μm) leads to annealing times greater than the age of the universe. Since film and vein lamellae coexist in these feldspars (as is usually the case) it is obvious that the processes of formation of the two intergrowths are different. Macroperthites with λ of several mm occur in some pegmatites and while we do not understand how such coarse periodic intergrowths form by replacement, the process is clearly not controlled by volume diffusion.

Microtextural work at higher magnification, using SEM and TEM, is required to understand the feldspars studied by Yuguchi and Nishiyama (2007) and Yuguchi et al. (2011a, 2011b), and the factors controlling the observed relationship between λ and position. A feature of both studies is that the Or contents stated for the Ab-rich phase in the film microperthites ($Ab_{60-80}Or_{40-20}$) are too high for equilibrium with an Or-rich phase at low *T*, because of the established asymmetry of the Ab-Or solvus. This, and the very large scatter of analyses of both Or- and Ab-rich phases, suggests that the spatial resolution of the EPMA analyses is inadequate, and that the microtextures are complex at sub-LM scales.

Implications and questions unanswered

In this review, we have attempted to summarize and critically assess features of alkali feldspars that have the potential to provide petrological and geochemical information, and to suggest the most practical means to access this information. Feldspars are intensely interesting in their own right and many other techniques have been used to study them, but the small subset of methods suggested here are those most likely to be used by non-specialists. We also submit, by reference to some recent publications, that care needs to be taken to reach reliable conclusions. Parsons (2010) lists nine major books on feldspars, four of them the outcomes of Advanced Study Institutes sponsored by NATO, from 1962 to 1994. These provide a fascinating (perhaps daunting) guide not only to the development of understanding of feldspars but also to the ever-increasing variety and sophistication of mineralogical techniques. The range of geological information that can be obtained from alkali feldspars is summarized here in the Introduction. Much of this information is missed in routine petrographic work and we hope this review will encourage petrologists to look a little more deeply at their feldspars, make more use of the techniques we recommend, and report what they find. Alkali feldspars make up 30% of the crust, mainly as a major constituent of granites, granulites and acid gneisses. Their microtextures record their history in the wide range of ways that we have summarized. As they end their lives, as detrital particles in sediments and soils, microtextures dictate the rate and mode of their destruction.

There are several areas of uncertainty for which we can see a way forward. In no particular order:

(1) We need to know more about the mechanisms, rates, and geochemical implications of replacement reactions. The overwhelming majority of alkali feldspars in plutonic rocks are, to variable extents turbid, and have therefore experienced replacement. How common is it for multiple phases of replacement to occur? What is the microtextural nature of the newly discovered ultra-porous late feldspar, with phase compositions very close to end-member, and how does it form in a piecemeal fashion, retaining "ghosts"of prexisting texture? Equally pure replacive subgrains can also form by a simple, apparently instantaneous process. What controls these different styles of replacement? How do these processes affect the major, trace element and isotopic chemistry of granitoids? If replacement is non-isochemical where do the introduced components come from and where do those lost go?

(2) A related problem is the regular periodicity of coarse vein perthites, often on scales of several hundred micrometers or even <100 mm. Such intergrowths are composed of subgrains and are clearly replacive. For kinetic reasons they cannot be accounted for by volume diffusion, although they may be directed by pre-existing coherent microtextures. How do such coarse periodic intergrowths form, and what do they tell us about *P-T-t* conditions?

(3) What is the thermodynamic character of the sanidine-microcline transformation? Is intermediate microcline a stable phase? What do the very large variety of twin microtextures in microcline tell us about its history? Are some replacive and some produced by volume diffusion? When microcline replaces orthoclase by an unzipping reaction how does it grow with increased order and with organized Albite and Pericline twins that retain the macroscopic monoclinic symmetry?

(4) Existing experimental work on the kinetics of coherent exsolution is restricted to An-free compositions. It is likely that exsolution is slowed because of coupling between Ca^{2+} and Al^{3+} but do higher exsolution *T* compensate? The microtextures are extremely fine-scale and TEM instrumentation and sample preparation methods have improved considerably since the pioneering work of Yund and co-workers in the 1970s.

(5) Two-feldspar geothermometry, although widely applied, still has uncertainties, particularly at low *T*. Direct synthesis work has well-known problems with attainment of equilibrium, and thermometers based on calorimetry should be developed for a wide range of compositions. A geothermometer could also be based on compressibility (equations of state) for a wide range of compositions. The question of the extreme effect of low concentrations of An on the ternary solvus for Or-rich feldspars is particularly interesting, because it is effectively caused by the relative incompressibility of anorthite compared with albite and sanidine.

Acknowledgments

We are indebted to Bill Brown (recently deceased), Alex McLaren, Richard Worden, Kim Waldron, David Walker, and Nicola Cayzer for providing EM images and insights that have contributed greatly to our understanding of alkali feldspar microtextures. We are also grateful for the support of four anonymous referees who recommended not only acceptance, but in two cases expansion, of an earlier, much shorter, version of this paper. We thank the Natural Environment Research Council for funding this research through grant NER/A/S/2003/00346.

References cited

Abart, R., Petrishcheva, E., Käßner, S., and Milke, R. (2009a) Perthite microstructure in magmatic alkali feldspar with oscillatory zoning; Weinsberg Granite, Upper Austria. Mineralogy and Petrology, 97, 251–263.

Abart, R., Petrishcheva, E., Wirth, R., and Rhede, D. (2009b) Exsolution by spi-

nodal decomposition II: Perthite formation during slow cooling of anatexites from Ngoronghoro, Tanzania. American Journal of Science, 309, 450–475.
Aberdam, D. (1965) Utilisation de la microscopie électronique pour l'étude des feldspaths. Observations sur des microperthites. Science de la Terre, 6, 1–76.
AlDahan, A.A., Morad, S., and Collini, B. (1987) Clouded-untwinned albite in the Siljan granite, central Sweden. Neues Jahrbuch für Mineralogie Monatshefte, 327–335.
Alling, H.L. (1921) The mineralography of the feldspars. Journal of Geology, 29, 193–294.
——— (1932) Perthites. American Mineralogist, 17, 43–65.
Andersen, O. (1928) The genesis of some types of feldspar from granite pegmatites. Norske Geologisk Tidskrift, 10, 116–207.
Bachinski, S.W., and Müller, G. (1971) Experimental determination of the microcline-low albite solvus. Journal of Petrology, 12, 329–356.
Balić-Žunić, T., Piazolo, S., Katerinopoulou, A., and Schmith, J.H. (2013) Full analysis of feldspar texture and crystal structure by combining X-ray and electron techniques. American Mineralogist, 98, 41–52.
Bambauer, H.U., Krause, C., and Kroll, H. (1989) TEM investigation of the sanidine/microcline transition across metamorphic zones. European Journal of Mineralogy, 1, 47–58.
Benisek, A., Dachs, E., and Kroll, H. (2010a) A ternary feldspar mixing model based on calorimetric data: development and application. Contributions to Mineralogy and Petrology, 160, 327–337.
——— (2010b) Excess heat capacity and entropy of mixing in the high-structural state (K,Ca)-feldspar binary. Physics and Chemistry of Minerals, 37, 209–218.
——— (2014) Thermochemistry of the alkali feldspars: Calorimetric study of the entropy relations in the low albite-low microcline series. American Mineralogist, 99, 76–83.
Bernotat-Wulf, H., Bertelmann, D., and Wondratschek, H (1988) The annealing behaviour of Eifel sanidine (Volkesfeld) III. The influence of the sample surface and sample size on the order-disorder transformation rate. Neues Jahrbuch für Mineralogie, Monatshefte, 504–515.
Bertelmann, D., Förtsch, E., and Wondratschek, H. (1985) Zum Temperverhalten von Sanidinen: Die Ausnahmerolle der Eifelsanidin-Megacrystal. Neues Jahrbuch für Mineralogie Abhandlungen, 152, 123–141.
Brady, J.B. (1987) Coarsening of fine-scale exsolution lamellae. American Mineralogist, 72, 697–706.
Brøgger, W.C. (1890) Die Mineralien der Syenitpegmatitgänge der südnorwegischen Augit- und Nephelinsyenite: 60 Albit. 61 Kryptoperthit. 61a Mikroperthit. 62 Mikroklin. Zeitschrift für Kristallographie, 16, 521–564.
Brown, W.L. (1993) Fractional crystallization and zoning in igneous feldspars: Ideal water-buffered liquid fractionation lines and feldspar zoning paths. Contributions to Mineralogy and Petrology, 113, 115–125.
Brown, W.L., and Parsons, I. (1981) Towards a more practical two feldspar geothermometer. Contributions to Mineralogy and Petrology, 76, 369–377.
——— (1984a) Exsolution and coarsening mechanisms and kinetics in an ordered cryptoperthite series. Contributions to Mineralogy and Petrology, 86, 3–18.
——— (1984b) The nature of potassium feldspar, exsolution microtextures and development of dislocations as a function of composition in perthitic alkali feldspars. Contributions to Mineralogy and Petrology, 86, 335–341.
——— (1985) Calorimetric and phase-diagram approaches to two-feldspar geothermometry: A critique. American Mineralogist, 70, 356–361.
——— (1988) Zoned ternary feldspars in the Klokken intrusion: Exsolution textures and mechanisms. Contributions to Mineralogy and Petrology, 98, 444–454.
——— (1989) Alkali feldspars: Ordering rates, phase transformations and behaviour diagrams for igneous rocks. Mineralogical Magazine, 53, 25–42.
——— (1993) Storage and release of elastic strain energy: The driving force for low temperature reactivity and alteration of alkali feldspars. In J.N. Boland and J.G. Fitz Gerald, Eds., Defects and Processes in the Solid State: Geoscience applications (The McLaren Volume), 267–290. Elsevier, Amsterdam.
——— (1994) Feldspars in igneous rocks. In I. Parsons, Ed., Feldspars and Their Reactions. NATO ASI Series, C 421, p. 449–499. Kluwer, Dordrecht.
Brown, W.L., Willaime, C., and Guillemin, C. (1972) Exsolution selon l'association diagonale dans une cryptoperthite: étude par microscopie électronique et diffraction des rayons X. Bulletin de la Societé francaise de Minéralogie (et Cristallographie), 95, 429–436.
Brown, W.L., Becker, S.M., and Parsons, I. (1983) Cryptoperthites and cooling rate in a layered syenite pluton. Contributions to Mineralogy and Petrology, 82, 13–25.
Buntebarth, G. (1991) Thermal models of cooling. In G. Voll, J. Töpel, D.R.M. Pattison, and F. Seifert, Eds., Equilbrium and Kinetics in Contact Metamorphism, p. 379–402. Springer-Verlag, Berlin.
Burgess, R., Kelley, S.P., Parsons, I., Walker, F.D.L., and Worden, R.H. (1992) ^{40}Ar-^{39}Ar analysis of perthite microtextures and fluid inclusions in alkali feldspars from the Klokken syenite, South Greenland. Earth and Planetary Science Letters, 109, 147–167.
Cahn, J.W. (1968) Spinodal decomposition. Transactions of the Metallurgical Society of AIME, 242, 166–180.
Carmichael, I.S.E. (1963) The crystallization of feldspar in volcanic acid liquids. Quarterly Journal of the Geological Society of London, 119, 95–131.
——— (1974) Igneous Petrology. McGraw-Hill, New York.
Carpenter, M.A. (1981) A "conditional spinodal" within the peristerite miscibility gap of plagioclase feldspars. American Mineralogist, 66, 553–560.
Carpenter, M.A., and Salje, E.K.H. (1994) Thermodynamics of nonconvergent cation ordering in minerals: III. Order parameter coupling in potassium feldspar. American Mineralogist, 79, 1084–1098.
Cayzer, N. (2002) Feldspar microtextures and the cooling histories of high-grade terrains. Unpublished Ph.D. thesis, University of Edinburgh, U.K.
Černý, P. (1994) Evolution of feldspars in granitic pegmatites. In I. Parsons, Ed., Feldspars and Their Reactions. NATO ASI Series, C 421, p. 501–540. Kluwer, Dordrecht.
Dietrich, R.V. (1962) K-feldspar structural states as petrogenetic indicators. Norsk Geologisk Tidsskrift, Bind 42, 2 Halvbind (Feldspar Volume), 394–414.
Eggleton, R.A., and Buseck, P.R. (1980) The orthoclase-microcline inversion: A high resolution transmission electron microscope study and strain analysis. Contributions to Mineralogy and Petrology, 74, 123–133.
Elkins, L.T., and Grove, T.L. (1990) Ternary feldspar experiments and thermodynamic models. American Mineralogist, 75, 544–559.
Engvik, A.K., Putnis, A., Fitz Gerald, J.D., and Austrheim, H. (2008) Albitization of granitic rocks: The mechanism of replacement of oligoclase by albite. Canadian Mineralogist, 46, 1401–1415.
Evangelakakis, C., Kroll, H., Voll, G., Wenk, H-R, Meisheng, H., and Köpcke, J. (1993) Low temperature coherent exsolution in alkali feldspars from high-grade metamorphic rocks of Sri Lanka. Contributions to Mineralogy and Petrology, 114, 519–532.
Ferry, J.M. (1985) Hydrothermal alteration of Tertiary igneous rocks from the Isle of Skye, northwest Scotland. Contributions to Mineralogy and Petrology, 91, 283–304.
Finch, A.A., and Klein, J. (1999) The causes and petrological significance of cathodoluminescence emission from alkali feldspars. Contributions to Mineralogy and Petrology, 135, 234–243.
Finch, A.A., Parsons, I., and Mingard, S.C. (1995) Biotites as indicators of fluorine fugacities in late stage magmatic fluids: The Gardar province, South Greenland. Journal of Petrology, 36, 1701–1728.
Fitz Gerald, J.D., and Harrison, T.M. (1993) Argon diffusion domains in K-feldspar I: microstructures in MH-10. Contributions to Mineralogy and Petrology, 113, 367–380.
Fitz Gerald, J.D., and McLaren, A.C. (1982) The microstructures of microcline from some granitic rocks and pegmatites. Contributions to Mineralogy and Petrology, 80, 219–229.
Fitz Gerald, J.D., Parsons, I., and Cayzer, N. (2006) Nanotunnels and pull-aparts: Defects of exsolution lamellae in alkali feldspars. American Mineralogist, 91, 772–783.
Fleet, S.G., and Ribbe, P. (1963) An electron-microscope investigation of a moonstone. Philosophical Magazine, 8, 1179–1187.
Flehmig, W. (1977) The synthesis of feldspars at temperatures between 0°–80°C, their ordering behaviour and twinning. Contributions to Mineralogy and Petrology, 65, 1–19.
Flude, S., Lee, M.R., Sherlock, S.C., and Kelley, S.P. (2012) Cryptic microtextures and geological histories of K-rich alkali feldspars revealed by charge contrast imaging. Contributions to Mineralogy and Petrology, 163, 983–994.
Fuhrman, M.L., and Lindsley, D.L. (1988) Ternary feldspar modelling and thermometry. American Mineralogist, 73, 201–215.
Goldich, S.S., and Kinser, J.H. (1939) Perthite from Tory Hill, Ontario. American Mineralogist, 24, 407–427.
Goldsmith, J.R., and Jenkins, D.M. (1985) The high-low albite relations revealed by reversal of degree of order at high pressure. American Mineralogist, 70, 911–923.
Götze, J., Krebetschek, M.R., Habermann, D., and Wolf, D. (2000) High resolution cathodoluminescence studies of feldspar minerals. In M. Pagel, V. Barbin, Ph. Blanc, and D. Ohnenstetter, Eds., Cathodoluminescence in Geosciences, p. 245–270. Springer-Verlag, Berlin.
Graham, C.M., and Elphick, S.C. (1990) A re-examination of the role of hydrogen in Al-Si interdiffusion in feldspars. Contributions to Mineralogy and Petrology, 104, 481–491.
Guidotti, C.V., Herd, H.H., and Tuttle, O.F. (1973) Composition and structural state of K-feldspars from K-feldspar + sillimanite grade rocks in Northwestern Maine. American Mineralogist, 58, 705–716.
Harker, R.I. (1954) The occurrence of orthoclase and microcline in the granitic gneisses of the Carn Chuinneag-Inchbae complex, E. Ross-shire. Geological Magazine, 91, 129–136.
——— (1962) The older orthogneisses of Carn Chuinneag and Inchbae. Journal of Petrology, 3, 215–237.
Harrison, T.N., Parsons, I., and Brown, P.E. (1990) Mineralogical evolution of fayalite-bearing rapakivi granites from the Prins Christians Sund pluton, South Greenland. Mineralogical Magazine, 54, 57–66.
Harrison, T.M., Heizler, M.T., McKeegan, K.D., and Schmitt, A.K. (2010) In situ ^{40}K-^{40}Ca "double-plus" SIMS dating resolves Klokken ^{40}K-^{40}Ar paradox. Earth and Planetary Science Letters, 299, 426–433.
Heaney, P.J., Vicenzi, E.P., Giannuzzi, L.A., and Livi, K.J.T. (2001) Focused ion beam milling: A method of site-specific sample extraction for microanalysis of Earth and planetary materials. American Mineralogist, 86, 1094–1099.
Hodson, M., Lee, M.R., and Parsons, I. (1997) Origins of the surface roughness of unweathered alkali feldspar grains. Geochimica et Cosmochimica Acta, 61, 3885–3896.
Hövelmann, J., Putnis, A., Geisler, T., Schmidt, B.C., and Golla-Schindler, U. (2010)

The replacement of plagioclase feldspars by albite: Observations from hydrothermal experiments. Contributions to Mineralogy and Petrology, 159, 43–59.
Hovis, G.L., Delbove, F., and Roll Bose, M. (1991) Gibbs energies and entropies of K-Na mixing for alkali feldspars from phase equilibrium data: Implications for feldspar solvi and short-range order. American Mineralogist, 76, 913–927.
Janney, D.E., and Wenk, H-R. (1999) Peristerite exsolution in metamorphic plagioclase from the Lepontine Alps: An analytical and transmission electron microscope study. American Mineralogist, 84, 517–527.
Johnson, E.A., and Rossman, G.R. (2004) A survey of hydrous species and concentrations in igneous feldspars. American Mineralogist, 89, 586–600.
Kroll, H., and Knitter, R. (1991) Al,Si exchange kinetics in sanidine and anorthoclase and modeling of rock cooling paths. American Mineralogist, 76, 928–941.
Kroll, H., and Ribbe, P.H. (1987) Determining (Al,Si) distribution and strain in alkali feldspars using lattice prameters and diffraction-peak positions. American Mineralogist, 72, 491–506.
Kroll, H., Krause, C., and Voll, G. (1991) Disordering, re-ordering and unmixing in alkali feldspars from contact-metamorphosed quartzites. In G. Voll, J. Töpel, D.R.M. Pattison, and F. Seifert, Eds., Equilibrium and Kinetics in Contact Metamorphism, p. 267–296. Springer-Verlag, Berlin.
Laves, F. (1950) The lattice and twinning of microcline and other potash feldspars. Journal of Geology, 58, 548–571.
Lee, M.R. (2010) Transmission electron microscopy (TEM) of Earth and planetary materials: A review. Mineralogical Magazine, 74, 1–27.
Lee, M.R., and Parsons, I. (1995) Microtextural controls of weathering of perthitic alkali feldspars. Geochimica et Cosmochimica Acta, 59, 4465–4488.
——— (1997a) Compositional and microtextural zoning in alkali feldspars from the Shap granite and its geochemical implications. Journal of the Geological Society of London, 154, 183–188.
——— (1997b) Dislocation formation and albitization in alkali feldspars from the Shap granite. American Mineralogist, 82, 557–570.
——— (1998) Microtextural controls of diagenetic alteration of detrital alkali feldspars: a case study of the Shap conglomerate (Lower Carboniferous), North-west England. Journal of Sedimentary Research, 68, 198–211.
——— (2003) Microtextures of authigenic Or-rich feldspar in the Upper Jurassic Humber Group, U.K. North Sea. Sedimentology, 50, 1–12.
Lee, M.R., Waldron, K.A., and Parsons, I. (1995) Exsolution and alteration microtextures in alkali feldspar phenocrysts from the Shap granite. Mineralogical Magazine, 59, 63–78.
Lee, M.R., Waldron, K.A., Parsons, I., and Brown, W.L. (1997) Feldspar-fluid interactions in braid microperthites: Pleated rims and vein microperthites. Contributions to Mineralogy and Petrology, 127, 291–304.
Lee, M.R., Hodson, M.E., and Parsons, I. (1998) The role of intragranular microtextures and microstructures in chemical and mechanical weathering: direct comparisons of experimentally and naturally weathered alkali feldspars. Geochimica et Cosmochimica Acta, 62, 2771–2788.
Lee, M.R., Bland, P.A., and Graham, G. (2003a) Preparation of TEM samples by focused ion beam (FIB) techniques: Applications to the study of clays and phyllosilicates in meteorites. Mineralogical Magazine, 67, 581–592.
Lee, M.R., Thompson, P., Poeml, P., and Parsons, I. (2003b) Peristeritic plagioclase in North Sea hydrocarbon reservoir rocks: Implications for diagenesis, provenance and stratigraphic correlation. American Mineralogist, 88, 866–875.
Lee, M.R., Brown, D.J., Smith, C.L., Hodson, M.E., MacKenzie, M., and Hellmann, R. (2007a) Characterization of mineral surfaces using FIB and TEM: A case study of naturally weathered alkali feldspars. American Mineralogist, 92, 1383–1394.
Lee, M.R., Parsons, I., Edwards, P., and Martin, R.W. (2007b) Identification of cathodoluminescence activators in zoned alkali feldspars by hyperspectral imaging and electron-probe microanalysis. American Mineralogist, 92, 243–253.
Lee, M.R., Hodson, M.E., Brown, D.J., MacKenzie, M., and Smith, C.L. (2008) The composition and crystallinity of the near-surface regions of weathered alkali feldspars. Geochimica et Cosmochimica Acta, 72, 4962–4975.
Lorimer, G.W., and Champness, P.E. (1973) The origin of the phase distribution in two perthitic alkali feldspars. Philosophical Magazine, 28, 1391–1403.
MacKenzie, W.S. (1957) The crystalline modifications of $NaAlSi_3O_8$. American Journal of Science, 255, 481–516.
MacKenzie, W.S., and Smith, J.V. (1962) Single crystal X-ray studies of crypto- and micro-perthites. Norsk Geologisk Tidsskrift, Bind 42, 2 Halvbind (Feldspar Volume), 72–103.
Marks, M., Vennemann, T., Siebel, W., and Markl, G. (2003) Quantification of magmatic and hydrothermal processes in a peralkaline syenite–alkali granite complex based on textures, phase equilibria, and stable and radiogenic isotopes. Journal of Petrology, 44, 1247–1280.
Martin, R.F. (1969) The hydrothermal synthesis of low albite. Contributions to Mineralogy and Petrology, 23, 323–339.
Mason, R.A. (1979) Ordering behaviour of albite in aqueous solutions at 1 kbar. Contributions to Mineralogy and Petrology, 68, 269–273.
——— (1980a) The ordering behaviour of reedmergnerite, $NaBSi_3O_8$. Contributions to Mineralogy and Petrology, 72, 329–333.
——— (1980b) Changes in the morphology of synthetic reedmergnerite ($NaBSi_3O_8$) during ordering experiments. Mineralogical Magazine, 43, 905–908.
——— (1982) Trace element distributions between the perthite phases of alkali feldspars from pegmatites. Mineralogical Magazine, 45, 101–106.
McDowell, S.D. (1986) Composition and structural state of coexisting feldspars, Salton Sea geothermal field. Mineralogical Magazine, 50, 75–84.
McLaren, A.C. (1974) Transmission electron microscopy of the feldspars. In W.S. MacKenzie, and J. Zussman, Eds., The Feldspars, p. 378–423. Manchester University Press, U.K.
McLaren, A.C., and Fitz Gerald, J.D. (1987) CBED and ALCHEMI investigation of local symmetry and Al, Si ordering in K-feldspars. Physics and Chemistry of Minerals, 14, 281–392.
McLaren, S., and Reddy, S.M. (2008) Automated mapping of K-feldspar by electron backscatter diffraction and application to $^{40}Ar/^{39}Ar$ dating. Journal of Structural Geology, 30, 1229–1241.
Menegon, L., Pennacchioni, G., and Spies, R. (2008) Dissolution–precipitation creep of K-feldspar in mid-crustal granite mylonites. Journal of Structural Geology, 30, 565–579.
Menegon, L., Stünitz, H., Nasipuri, P., Heilbronner, R., and Svanberg, H. (2013) Transition from fracturing to viscous flow in granulite facies perthitic feldspar (Lofoten, Norway). Journal of Structural Geology, 48, 95–112.
Müller, G. (1971) Der Einfluss der Al,Si-Verteilung auf die Mischungslücke der Alkali feldspäte. Contributions to Mineralogy and Petrology, 34, 73–79.
Nakano, S. (1998) Calcium distribution patterns in alkali feldspar in a quartz syenite from Oki-Dozen, southwest Japan. Mineralogy and Petrology, 63, 35–48.
Nakano, S., Akai, J., and Shimobayashi, N. (2005) Contrasting Fe-Ca distributions and related microtextures in syenite alkali feldspar from the Patagonian Andes, Chile. Mineralogical Magazine, 69, 521–536.
Norberg, N., Neusser, G., Wirth, R., and Harlov, D. (2011) Microstructural evolution during experimental albitization of K-rich alkali feldspar. Contributions to Mineralogy and Petrology, 162, 531–546.
Norberg, N., Harlov, D., Neusser, G., Wirth, R., Rhede, D., and Morales, L. (2013) Experimental development of patch perthite from synthetic cryptoperthite: Microstructural evolution and chemical re-equilibration. American Mineralogist, 98, 1429–1441.
Parsons, I. (1965) The feldspathic syenites of the Loch Ailsh intrusion, Assynt, Scotland. Journal of Petrology, 6, 365–394.
——— (1978) Feldspars and fluids in cooling plutons. Mineralogical Magazine, 42, 1–17.
——— (1980) Alkali feldspar and Fe-Ti oxide exsolution textures as indicators of he distribution and subsolidus effects of magmatic "water" in the Klokken layered syenite intrusion, South Greenland. Transactions of the Royal Society of Edinburgh: Earth Sciences, 71, 1–12.
——— (2010) Feldspars defined and described: a pair of posters published by the Mineralogical Society. Sources and supporting information. Mineralogical Magazine, 74, 529–551.
Parsons, I., and Becker, S.M. (1986) High temperature fluid-rock interactions in a layered syenite pluton. Nature, 321, 764–769.
Parsons, I., and Boyd, R. (1971) Distribution of potassium feldspar polymorphs in intrusive sequences. Mineralogical Magazine, 38, 295–311.
Parsons, I., and Brown, W.L. (1983) A TEM and microprobe study of a two-perthite alkali gabbro: Implications for the ternary feldspar system. Contributions to Mineralogy and Petrology, 82, 1–12.
——— (1984) Feldspars and the thermal history of igneous rocks. In W.L. Brown, Ed., Feldspars and Feldspathoids: Structure, properties and occurrences. NATO ASI Series C, vol. 137, p. 317–371. Reidel, Dordrecht.
——— (1991) Mechanisms and kinetics of exsolution—Structural control of diffusion and phase behavior in alkali feldspars. In J. Ganguly, Ed., Diffusion, Atomic Ordering, and Mass Transport. Advances in Physical Geochemistry, 9, p. 306–346. Springer-Verlag, Berlin.
Parsons, I., and Fitz Gerald, J.D. (2011) Coarsening kinetics of coexisting peristerite and film microperthite over 10^4 to 10^5 years. American Mineralogist, 96, 1575–1584.
Parsons, I., and Lee, M.R. (2005) Minerals are not just chemical compounds. Canadian Mineralogist, 43, 1959–1992.
——— (2009) Mutual replacement reactions in alkali feldspars I: Microtextures and mechanisms. Contributions to Mineralogy and Petrology, 157, 641–661.
Parsons, I., Rex, D.C., Guise, P., and Halliday, A.N. (1988) Argon-loss by alkali feldspars. Geochimica et Cosmochimica Acta, 52, 1097–1112.
Parsons, I., Lee, M.R., and Smith, J.V. (1998) Biochemical evolution: II. Origin of life in tubular microstructures on weathered feldspar surfaces. Proceedings of the National Academy of Sciences, 95, 15173–15176.
Parsons, I., Brown, W.L., and Smith, J.V. (1999) $^{40}Ar/^{39}Ar$ thermochronology using alkali feldspars: Real thermal history of mathematical mirage of microtexture. Contributions to Mineralogy and Petrology, 136, 92–110.
Parsons, I., Thompson, P., Lee, M.R., and Cayzer, N. (2005) Alkali feldspar microtextures as provenance indicators in siliciclastic rocks and their role in feldspar dissolution during transport and diagenesis. Journal of Sedimentary Research, 75, 921–942.
Parsons, I., Steele, D., Lee, M.R., and Magee, C. (2008) Titanium as a cathodoluminescence activator in alkali feldspars. American Mineralogist, 93, 875–879.
Parsons, I., Magee, C., Allen, C., Shelley, M.J., and Lee, M.R. (2009) Mutual replacement reactions in alkali feldspars II: Trace element partitioning and geothermometry. Contributions to Mineralogy and Petrology, 157, 663–687.

Parsons, I., Fitz Gerald, J.D., Lee, J.K.W., Ivanic, T., and Golla-Schindler, U. (2010) Time-temperature evolution of microtextures and contained fluids in a plutonic alkali feldspar during heating. Contributions to Mineralogy and Petrology, 160, 155–180.

Parsons, I., Fitz Gerald, J.D., Heizler, M.T., Heizler, L.L., Ivanic, T., and Lee, M.R. (2013) Eight-phase alkali feldspars: Low-temperature cryptoperthite, peristerite and multiple replacement reactions in the Klokken intrusion. Contributions to Mineralogy and Petrology, 165, 931–961.

Plümper, O., and Putnis, A. (2009) The complex hydrothermal history of granitic rocks: Multiple feldspar replacement reactions under subsolidus conditions. Journal of Petrology, 50, 967–987.

Presnall, D.C., and Bateman, P.C. (1973) Fusion relations in the system $NaAlSi_3O_8$–$CaAl_2Si_2O_8$–$KAlSi_3O_8$–SiO_2–H_2O and generation of granitic magmas in the Sierra Nevada batholith. Geological Society of America Bulletin, 84, 3181–3202.

Prior, D.J., and Wheeler, J. (1999) Feldspar fabrics in a greenschist facies albite-rich mylonite from electron backscatter diffraction. Tectonophysics, 303, 29–49.

Prior, D.J., Boyle, A.P., Brenker., F., Cheadle, M.C., Day, A., Lopez, G., Peruzzo, L., Potts, G.J., Reddy, S., Spiess, R., and others. (1999) The application of electron backscatter diffraction and orientation contrast imaging in the SEM to textural problems in rocks. American Mineralogist, 84, 1741–1759.

Putnis, A. (2002) Mineral replacement reactions: from macroscopic observations to microscopic mechanisms. Mineralogical Magazine, 66, 689–708.

Putnis, A., and Salje, E. (1994) Tweed microstructures: Experimental observations and some theoretical models. Phase Transitions, 48, 85–105.

Putnis, A., Hinrichs, R., Putnis, C.V., Golla-Schindler, U., and Collins, L.G. (2007) Hematite in porous red-clouded feldspars: Evidence of large-scale fluid-rock interaction. Lithos, 95, 10–18.

Ramseyer, K., AlDahan, A.A., Collini, B., and Landström, O. (1992) Petrological modifications in granitic rocks from the Siljan impact structure: Evidence from cathodoluminescence. Tectonophysics, 216, 195–204.

Ribbe, P.H. (1979) The structure of a strained intermediate microcline in cryptoperthitic association with twinned plagioclase. American Mineralogist, 64, 402–408.

Rosenqvist, I.T. (1965) Electron-microscope investigations of larvikite and tönsbergite feldspars. Norsk Geologisk Tidsskrift, 45, 69–71.

Robin, P.-Y.F. (1974) Stress and strain in cryptoperthite lamellae and the coherent solvus of alkali feldspars. American Mineralogist, 59, 1299–1318.

Sánchez-Muñoz, L., García-Guinea, J., Zagorsky, V. Ye., Juwong, T., Modreski, P.J., Cremades, A., Van Tendeloo, G., and De Moura, O.J.M. (2012) The evolution of twin patterns in perthitic K-feldspar from granitic pegmatites. Canadian Mineralogist, 50, 989–1024.

Scott, R.B., Bachinski, S.W., Nesbitt, R.W., and Scott, M.R. (1971) Rate of Al-Si ordering in sanidines from an ignimbrite cooling unit. American Mineralogist, 56, 1208–1221.

Short, C.H., Heizler, M.T., Parsons, I., amd Heizler, L. (2011) MDD analysis of microtexturally characterized K-feldspar fragments. American Geophysical Union Fall Meeting, San Francisco, California. Abstract V23A-2553.

Sipling, P.J., and Yund, R.A. (1976) Experimental determination of the coherent solvus for sanidine-high albite. American Mineralogist, 61, 897–906.

Słaby, E., Martin, H., Hamada, M., Śmigielski, M., Domonik, A., Götze, J., Hoefs, J., Hałas, S., Simon, K., Devidal, J.-L., Moyen, J.-F., and Jayananda, M. (2012) Evidence in Archaean alkali feldspar megacrtsts for high-temperature interaction with mantle fluids. Journal of Petrology, 53, 67–98.

Smith, J.V. (1974) Feldspar Minerals, first edition, volume 1, p. 627. Springer-Verlag, Berlin.

——— (1994) Surface chemistry of feldspars. In I. Parsons, Ed., Feldspars and Their Reactions. NATO ASI Series C, p. 541–594. Kluwer, Dordrecht.

Smith, J.V., and Brown, W.L. (1988) Feldspar Minerals, second edition, volume 1, p. 828. Springer-Verlag, Berlin.

Smith, J.V., and MacKenzie, W.S. (1955) The alkali feldspars: II. A simple X-ray technique for the study of alkali feldspars. American Mineralogist, 40, 733–747.

Smith, K.L., and McLaren, A.C. (1983) TEM investigation of a microcline from a nepheline syenite. Physics and Chemistry of Minerals, 10, 69–76.

Smith, P., and Parsons, I. (1974) The alkali feldspar solvus at 1 kilobar water vapour pressure. Mineralogical Magazine, 39, 747–767.

Stewart, D.B., and Wright, T.L. (1974) Al/Si order and symmetry of natural alkali feldspars, and the relationship of strained cell parameters to bulk composition. Bulletin de la Societé francaise de Minéralogie (et Cristallographie), 97, 356–377.

Su, S-C., Ribbe, P.H., and Bloss, F.D. (1986) Alkali feldspars: structural state determined from composition and optic axial angle $2V$. American Mineralogist, 71, 1285–1296.

Tajčmanová, L., Abart, R., Wirth, R., Habler, G., and Rhede, D. (2012) Intracrystalline microstructures in alkali feldspars from fluid-deficient felsic granulites: A mineral chemical and TEM study. Contributions to Mineralogy and Petrology, 164, 715–729.

Taroev, V., Göttlicher, J., Kroll, H., Kashaev, A., Suvarova, L., Pentinghaus, H., Bernotat-Wulff, H., Breit, U., Tauson, V., and Lashkevich, V. (2008) Synthesis and structural state of K-feldspars in the system K [$AlSi_3O_8$]–K [$FeSi_3O_8$]. European Journal of Mineralogy, 20, 635–651.

Tuttle, O.F., and Bowen, N.L. (1958) The origin of granite in the light of experimental studies in the system $NaAlSi_3O_8$-$KAlSi_3O_8$-SiO_2-H_2O. Geological Society of America Memoir 74, p. xi+133.

Wahlgren, C-H., Ahl, M., Sandahl, K.-A., Berglund, J., Petersson, J., Ekström, M., and Persson, P.-O. (2004) Bedrock mapping 2003—Simpevarp subarea. Outcrop data, fracture data, modal and geochemical classification of rock types, bedrock map, radiometric dating. Okershamm site investigation. SKB P-04-102. Svenska Kärnbränlehantering AB.

Waldron, K.A., and Parsons, I. (1992) Feldspar microtextures and multistage thermal history of syenites from the Coldwell Complex, Ontario. Contributions to Mineralogy and Petrology, 111, 222–234.

Waldron, K.A., Parsons, I., and Brown, W.L. (1993) Solution-redeposition and the orthoclase-microcline transformation: evidence from granulites and relevance to ^{18}O exchange. Mineralogical Magazine, 57, 687–695.

Waldron, K.A., Lee, M.R., and Parsons, I. (1994) The microstructures of perthitic alkali feldspars revealed by hydrofluoric acid etching. Contributions to Mineralogy and Petrology, 116, 360–364.

Walker, F.D.L. (1991) Micropores in alkali feldspars. Unpublished Ph. D thesis, University of Edinburgh, U.K.

Walker, F.D.L., Lee, M.R., and Parsons, I. (1995) Micropores and micropermeable texture in alkali feldspars: Geochemical and geophysical implications. Mineralogical Magazine, 59, 505–534.

Wen, S.X., and Nekvasil, H. (1994) Solvcalc—An interactive graphics program package for calculating the ternary feldspar solvus and for 2-feldspar geothermometry. Computers and Geosciences, 20, 1025–1040.

Willaime, C., and Brown, W.L. (1974) A coherent elastic model for the determination of the orientation of exsolution boundaries: Application to the feldspars. Acta Crystallographica A, 30, 313–331.

Willaime, C., and Gandais, M. (1972) Study of exsolution in alkali feldspars. Calculation of elastic stresses inducing periodic twins. Physica Status Solidi a, 9, 529–539.

Wirth, R. (2004) Focused Ion Beam (FIB): A novel technology for advanced application of micro- and nanoanalysis in geosciences and applied mineralogy. European Journal of Mineralogy, 16, 863–876.

Worden, R.H., and Rushton, J.C. (1992) Diagenetic K-feldspar textures: A TEM study and model for diagenetic feldspar growth. Journal of Sedimentary Petrology, 62, 779–789.

Worden, R.H., Walker, F.D.L., Parsons, I., and Brown, W.L. (1990) Development of microporosity, diffusion channels and deuteric coarsening in perthitic alkali feldspars. Contributions to Mineralogy and Petrology, 104, 507–515.

Yuguchi, T., and Nishiyama, T. (2007) Cooling process of a granitic body deduced from the extents of exsolution and deuteric sub-solidus reactions: Case study of the Okueyama granitic body, Kyushu, Japan. Lithos, 97, 395–421.

Yuguchi, T., Tsuruta, T., and Nishiyama, T. (2011a) Three-dimensional cooling pattern of a granitic pluton I: The study of exsolution sub-solidus reactions in the Toki granite, Central Japan. Journal of Mineralogical and Petrological Sciences, 106, 61–78.

——— (2011b) Three-dimensional cooling pattern of a granitic pluton II: The study of deuteric sub-solidus reactions in the Toki granite, Central Japan. Journal of Mineralogical and Petrological Sciences, 106, 130–141.

Yund, R.A. (1974) Coherent exsolution in the alkali feldspars. In A.W. Hofmann, B.J. Giletti, H.S. Yoder Jr., and R.A. Yund, Eds., Geochemical Transport and Kinetics, 634, p. 173–184. Carnegie Institution of Washington Publication.

——— (1984) Alkali feldspar exsolution: Kinetics and dependence on alkali interdiffusion. In W.L. Brown, Ed., Feldspars and Feldspathoids. NATO ASI Series C, vol. 137, p. 281–315. Reidel, Dordrecht.

Yund, R.A., and Davidson, P. (1978) Kinetics of lamellar coarsening in cryptoperthites. American Mineralogist, 63, 470–477.

Zeipert, C., and Wondratschek, H. (1981) An unusual annealing behaviour of Eifel sanidine. Neues Jahrbuch für Mineralogie Monatshefte, 407–415.

Zeitler, P.K., Chamberlain, C.P., and Smith, H.A. (1993) Synchronous anatexis, metamorphism, and rapid denudation at Nanga Parbat (Pakistan Himalaya). Geology, 21, 347–350.

Manuscript received June 13, 2014
Manuscript accepted November 8, 2014
Manuscript handled by Lars Ehm